

**THE UNIVERSITY OF WESTERN ONTARIO  
DEPARTMENT OF CIVIL AND  
ENVIRONMENTAL ENGINEERING**

**Water Resources Research Report**

**Assessment of uncertainty in flood flows under  
climate change: the Upper Thames River  
Basin (Ontario, Canada)**

**By:**

**Samiran Das  
and  
Slobodan P. Simonovic**

**Report No: 079  
Date: March 2012**

**ISSN: (print) 1913-3200; (online) 1913-3219;  
ISBN: (print) 978-0-7714-2960-6; (online) 978-0-7714-2961-3;**



Assessment of uncertainty in flood flows under climate change - the Upper  
Thames River basin (Ontario, Canada)

Samiran Das and Slobodan P. Simonovic

Department of Civil and Environmental Engineering, University of Western Ontario, London  
Ontario, N6A5B9, Canada

## **Abstract**

The assessment of climate change impacts on frequency and magnitude of flood flows is important for flood risk management. It is recognized that existing methods for the assessment of climate change impacts are subject to various sources of uncertainty (choice of climate model, choice of emission scenario, course spatial and temporal scales, etc.).

This study investigates the climate change related uncertainty in the flood flows for the Upper Thames River basin (Ontario, Canada) using a wide range of climate model scenarios. Fifteen different climate model scenarios from a combination of six Atmosphere-Ocean Global Climate Models (AOGCMs) and three emission scenarios “A1B”, “B1” and “A2” out of the family of emission scenarios are used to determine an uncertainty envelope of future estimated flood flows.

In this study, AOGCM data is downscaled using the change factor approach for 30-year time slices centered on years 2020, 2050 and 2080. To estimate natural variability, a stochastic weather generator is used to produce synthetic time series for each horizon and for each climate change scenario. The weather generator is also used to perturb historical data so that a number of realizations can be produced for the 1979-2005 baseline.

A continuous daily hydrologic model, calibrated for the basin, was then used to generate daily flow series for the 1979-2005 baseline period and the 2020, 2050 and 2080s. A peak-over-threshold (POT) modeling approach with Generalized Pareto Distribution is used to produce flood frequency distributions for the four time horizons. The uncertainty involved with the POT modelling is also considered.

The results indicate that frequency and magnitude of flood flows in the Upper Thames River basin will most certainly change in the future due to climate change. Inherent uncertainties associated with different AOGCMs are quantified by a normal kernel function. Use of a probability based frequency curve is encouraged in order to apply the flood magnitude-return period relationship with high level of confidence.

# Table of Contents

Abstract.....	ii
Table of Contents.....	iii
List of Tables.....	iv
List of Figures.....	v
1 Introduction.....	1
1.1 Research Problem.....	1
1.2 Objective of the Study.....	3
1.3 Approach.....	3
1.4 Organization of the Report.....	4
2 Literature Review.....	5
3 Methodology.....	7
3.1 Climate Models.....	7
3.2 Weather Generator.....	8
3.3 Hydrological Model.....	11
3.3.1 Model Structure.....	11
3.3.2 Snow Module.....	13
3.3.3 Losses Module.....	14
3.3.4 Transform and Routing Modules.....	15
3.4 Statistical Analysis.....	16
3.4.1 POT Modelling:.....	16
3.4.2 Generalized Pareto Distribution (GPD).....	17
3.4.3 Selection of Peaks.....	18

3.4.4	Test of Suitability of GPD Distribution: L-Moment Ratio Diagrams .....	19
3.4.5	Test of Poisson Process .....	20
4	Case Study .....	22
4.1	Description of the Watershed.....	22
4.2	Hydrological Model Setup, Calibration and Validation.....	25
4.3	Data Source and Production of POT Series.....	27
5	Results and Discussions .....	29
5.1	Peak Flows.....	29
5.2	Evaluation of POT Modelling.....	31
5.2.1	Suitability of GPD Distribution .....	31
5.2.2	Poisson Process .....	32
5.2.3	Shape Parameter Uncertainty.....	33
5.3	Flood Magnitude - Return Period Relationship and Uncertainties.....	34
6	Conclusions.....	45
	Acknowledgements.....	46
	References.....	47
	APPENDIX A.....	51
	APPENDIX B .....	55

## List of Tables

Table 3.1	List of AOGCM models and emission scenarios used .....	7
Table 4.1	Location of stations in the Upper Thames River basin.....	24
Table 5.1	Percentage of rejections at the 5% significance level for the dispersion test .....	33

## List of Figures

Figure 3.1 Continuous hydrologic model structure .....	12
Figure 3.2 Soil moisture accounting losses module.....	15
Figure 4.1 Map of the Upper Thames River basin.....	23
Figure 4.2 Schematic of Upper Thames River basin hydrologic models (Prodanovic and Simonovic, 2006).....	26
Figure 5.1 Box-plots of peak discharges for all AOGCMs considered in this study. Results are for the Byron gauging station in the Upper Thames River basin at the 2020, 2050 and 2080 time horizons. The baseline period (BL) is also included with each future time horizon.....	30
Figure 5.2 L-moment ratio diagrams for POT series obtained for all future climate projections, and for the baseline period (BL).....	32
Figure 5.3 Box plots of shape parameter of GPD distribution at the four time horizons .....	34
Figure 5.4 Simulated flood frequency results for climate data at time horizon 2020. Data from 375 scenarios (15 climate model scenarios x 25 model runs each) are used. Each line with a specific color represents a different AOGCM. The upper and lower bound frequency curves are obtained from scenario runs derived from CGCM3T63-A2 and MICRO3HIRES-B1, respectively.....	35
Figure 5.5 Simulated flood frequency results for climate data at time horizon 2050. Data from 375 scenarios (15 climate model scenarios x 25 model runs each) are used. Each line with a specific color represents a different AOGCM. The upper and lower bound frequency curves are obtained from scenario runs derived from MICRO3MEDRES-A2 and MICRO3MEDRES-A1B, respectively.....	36
Figure 5.6 Simulated flood frequency results for climate data at time horizon 2080. Data from 375 scenarios (15 climate model scenarios x 25 model runs each) are used. Each line with a specific color represents a different AOGCM. The upper and lower bound frequency curves are obtained from scenario runs derived from CGCM3T63-A2 and MICRO3MEDRES-A1B, respectively. ....	36
Figure 5.7 Simulated flood frequency results for climate data at baseline. Data from 25 runs produced a range of results.....	37

Figure 5.8 Simulated flood frequency results for climate data at time horizon 2020. Data from 150 scenarios (6 Canadian climate model scenarios x 25 model run each) are used. The upper and lower bound frequency curves are obtained from scenario runs derived from CGCM3T63-A2 and CGCM3T47-A1B, respectively.....	38
Figure 5.9 Simulated flood frequency results for climate data at time horizon 2050. Data from 150 scenarios (6 Canadian climate model scenarios x 25 model run each) are used. The upper and lower bound frequency curves are obtained from scenario runs derived from CGCM3T63-A2 and CGCM3T47-A1B, respectively.....	38
Figure 5.10 Simulated flood frequency results for climate data at time horizon 2080. Data from 150 scenarios (6 Canadian climate model scenarios x 25 model run each) are used. The upper and lower bound frequency curves are obtained from scenario runs derived from CGCM3T63-A1B and CGCM3T63-B1, respectively.....	39
Figure 5.11 Probability density functions (PDFs) of 100-year return period flood for all AOGCMs at the time horizon 2050. Each PDF is constructed using 25 model runs.....	40
Figure 5.12 Probability density plots for 10-year return period flood for the four time horizons.....	41
Figure 5.13 Probability density plots for 100-year return period flood for the four time horizons. ....	41
Figure 5.14 Probability density plots for 250-year return period flood for the four time horizons. ....	42
Figure 5.15 CDFs for 10-year return period flood for the four time horizons.....	42
Figure 5.16 CDFs for 100-year return period flood for the four time horizons.....	43
Figure 5.17 CDFs for 250-year return period flood for the four time horizons.....	43
Figure A. 1 Probability density functions for 10-year return period flood for all climate model scenarios at the time horizon 2020. ....	51
Figure A. 2 Probability density functions for 100-year return period flood for all climate model scenarios at the time horizon 2020. ....	51
Figure A. 3 Probability density functions for 250-year return period flood for all climate model scenarios at the time horizon 2020. ....	52
Figure A. 4 Probability density functions for 10-year return period flood for all climate model scenarios at the time horizon 2050. ....	52
Figure A. 5 Probability density functions for 250-year return period flood for all climate model scenarios at the time horizon 2050. ....	53
Figure A. 6 Probability density functions for 10-year return period flood for all climate model scenarios at the time horizon 2080. ....	53

Figure A. 7 Probability density functions for 100-year return period flood for all climate model scenarios at the time horizon 2080. .... 54

Figure A. 8 Probability density functions for 250-year return period flood for all climate model scenarios at the time horizon 2080. .... 54

# **1 Introduction**

## **1.1 Research Problem**

It is widely recognized that hydrologic cycle will be intensified by increasing global temperatures, resulting from increased anthropogenic emissions of carbon dioxide. This will influence climate variables and will result in changes in climate. One of the expected consequences of climate change is increase in the magnitude and frequency of extreme hydrologic events (IPCC, 2007). A number of studies in the Canadian context concur with the findings of IPCC (2007). Notably, a study performed by the Environment Canada (EC, 2007) on four selected river basins in Ontario using a modeling exercise, indicates that the impacts of future climate change on the frequency and magnitude of precipitation, stream flow, and associated flooding risks will increase in that part of Canada. It is also reported that the monthly total number of rainfall related water damage insurance claims and incurred loss could increase by about 20% to 30% in the 2nd half of the 21st century. Also, the assessment of the vulnerability of Canadian public infrastructure to changing climatic conditions performed by the Public Infrastructure Engineering Vulnerability Committee of Engineers Canada (PIEVC, 2008), concludes that the failures of water resource's infrastructure due to climate change will become increasingly common across Canada. It is suggested among others, by Simonovic (2008) that water resource's infrastructure design criteria should be revised to adapt to the expected changes in magnitude and frequency of extreme events.

The climate change impact assessments of extremes such as floods are of particular interest because floods usually have the greatest and most direct impact on our everyday lives, community and environment. Changes in the frequency of flooding events are expected and projected changes will have serious implications for planning, operation and design of water resources systems. However, quantifying the changes in extremes is subject to various sources of uncertainty and hence requires further investigation.

Assessment of climate change impacts on floods incorporates projection of climate variables into a global scale, downscaling of global scale climatic variables into local scale hydrologic

variables and computations of risk of future extreme floods for purposes of water resources planning and management. Global scale climate variables are commonly projected by Coupled Atmosphere-Ocean Global Climate Models (AOGCMs), which provide a numerical representation of climate systems based on the physical, chemical and biological properties of their components and feedback interactions between these (IPCC, 2007). These models are current state of the art in climate change research and they are the most reliable tools available for describing the physics and chemistry of the atmosphere and oceans and for deriving projections of meteorological variables (temperature, precipitation, wind speed, solar radiation, humidity, pressure, etc). They are based on various assumptions about the effects of the concentration of greenhouse gases in the atmosphere coupled with projections of CO<sub>2</sub> emission rates (Smith et al., 2009). There is a high degree of consensus in the scientific community that AOGCMs are able to capture large scale circulation patterns and correctly model varying fields, such as surface pressure, especially at continental or larger scales. However, it is extremely unlikely that these models properly reproduce highly variable fields, such as precipitation, on a regional scale (Hughes and Guttorp, 1994).

A single AOGCM have been used by most of the studies related to climate change impacts for predicting future climate. It is recognized that there is a great deal of uncertainty involved in the estimation of future extreme floods under climate change (e.g. Prudhomme et al., 2003; Mareuil et al., 2006; Minville, 2008). The utilization of a single AOGCM may only represent a single realization out of a multiplicity of possible realizations and therefore cannot be representative of future. Therefore, for a reliable assessment of future changes in extremes, it is important to use collective information by utilizing all available climate models and by synthesizing the projections and uncertainties in a probabilistic manner.

## **1.2 Objective of the Study**

The study is concerned with the assessment of climate change impacts on floods. The traditional way to address the problem is to develop climate scenarios from the GCMs and link the scenarios to a hydrological model from which peak flow values are extracted and analysed. It is recognized that existing methods for the assessment of climate change impacts are subject to various sources of uncertainty (choice of climate model, choice of emission scenario, course spatial and temporal scales, etc.).

The main objective of the study is to investigate the climate change related uncertainty in the estimation of extreme flood flows for the Upper Thames River basin (Ontario, Canada) using a wide range of climate model scenarios. The peak over threshold (POT) approach of flood frequency is considered in this study to estimate flood magnitude - return period (Q-T) relationship. The study also address the suitability of the distributions associated with the POT model, and the uncertainty involved with the POT modelling under climate change.

## **1.3 Approach**

The approach considers the following steps:

1. Climate data is obtained from several AOGCMs. Fifteen different climate model scenarios from a combination of six Atmosphere-Ocean Global Climate Models (AOGCMs) and three emission scenarios “A1B”, “B1” and “A2” out of the family of emission scenarios are considered in this study.
2. AOGCM data is downscaled using a stochastic weather generator. The change factors for 30-year time slices centered on years 2020, 2050 and 2080 are calculated first. The change factors are then used to modify the historic datasets. Synthetic time series, for each time horizon and for each climate change scenario, are derived by using the modified historic data sets as input to the weather generator. Baseline scenario (1979-

2005) is produced by perturbing historical data using the weather generator. In each case (15 AOGCMs and baseline) 25 model runs are performed.

3. The hydrological simulations are carried out in a continuous mode using the HEC-HMS model and
4. The peak flows are obtained and hydrological impacts of climate change are assessed through the flood frequency peak over threshold (POT) approach.

#### **1.4 Organization of the Report**

The outline of the report is organised as follows. Chapter 2 presents literature relevant to the development of methods for assessing climate change impacts on flood flows. Chapter 3 describes the methodology applied in this study. Chapter 4 describes the study area of The Upper Thames River basin (UTRb), along with the production of POT series for the Byron gauging station. Chapter 4 presents and discusses the results. Finally the study is concluded in Chapter 5.

## 2 Literature Review

The assessment of climate change impacts on flood flows is generally conducted by linking climate scenarios, usually precipitation and air-temperature outputs from GCMs, to a deterministic hydrological model to simulate river flows, from which peak flows are assessed through a flood frequency approach. For instance, Roy et al. (2001) used daily precipitation and temperature values extracted from the Canadian coupled global climate model 1 (CGCM1) as input values to a lumped hydrological model to investigate the effect of climate change on peak discharges of the Chateaugay River, Canada. Loukas et al. (2002) also used output values from the CGCM1 model, linked to the UBC watershed model to simulate the discharge of two mountainous watersheds located in different climatic regions of BC, Canada. POT series were extracted from simulated flows for frequency analysis in the study by Loukas et al. (2002).

It is recognized that the above methods for the assessment of climate change impacts are subject to various sources of uncertainty. The uncertainty mainly depends on climate data (choice of climate model, choice of emission scenario) and simulated hydrologic regimes (Prudhomme et al., 2003). Prudhomme et al. (2003) address the problem to some extent (climate related uncertainty) by generating a large ensemble of climate scenarios using Monte Carlo simulation. Their study used change factor approach to produce large ensemble of climate scenarios. Results from a single scenario were discouraged in their study. They suggested rather a range of climate scenarios derived from different GCMs should be considered in climate change impact studies.

A more recent approach of incorporating uncertainty due to climate data in hydrological impact studies is to use several climate projections obtained from the combinations of GCM and emission scenarios. For example, Minville (2008) in their study for the assessment of impact of climate change on the hydrology of the Chute-du-Diable watershed (Quebec, Canada), used 10 climate projections from a combination of 5 general circulation models (GCMs) and 2 greenhouse gas emission scenarios. Mareuil et al. (2006) used three GCMs to account for uncertainties related to the internal structure of the GCMs. Their study focused on the potential effects of climate change on the flood frequency and severity in a watershed subjected to spring

snowmelt and summer-fall storms. In both studies, POT series were derived through a continuous hydrological model driven by GCM-derived climate scenarios for frequency analysis. Kay et al. (2006, 2009) also performed similar kind of studies for UK catchments.

The consideration of large number of climate models and scenarios also permits a probabilistic assessment of future flood flow uncertainty. The probabilistic treatment of climate related uncertainty was performed in many recent studies. Other than simple normal assumption several techniques are explored by researchers: for example, Giorgi and Mearns (2003) used ‘Reliability Ensemble Averaging (REA)’ technique, Tebaldi et al. (2004; 2005) introduced a Bayesian treatment of ‘Reliability Ensemble Averaging (REA)’ approach and, Ghosh and Mujumdar (2007) and Solaiman and Simonovic (2011) used a non-parametric approach to quantify uncertainty of hydrologic variables in climate change impact studies. Probabilistic approach thus appeared to be an important platform for estimating uncertainties from multi-model outputs.

### 3 Methodology

This section details the methodology applied in the study which includes use of different types of AOGCM models and emission scenarios, weather generator model, continuous hydrological model and statistical models.

#### 3.1 Climate Models

Global circulation models namely, coupled Atmosphere-Ocean Global Climate Models (AOGCMs) are current state of the art in climate change research. AOGCMs are the most viable tools for simulating physical processes in the atmosphere, ocean, cryosphere and land surface that determine global climate (IPCC, 2007). AOGCMs are associated with model structure developed by various countries, and the emission scenarios. Three emission scenarios “A1B”, “B1” and “A2” out of the family of emission scenarios (Nakićenović and Swart, 2000) are most commonly used in climate impact studies. These represent respectively “the productive world with rapid economic expansion and abundance of energy sources”, “the sustainable world with clean technologies” and “the world of independent nations with increasing population and slower technological advancements”, respectively. In this study, a total of 15 scenarios from 6 AOGCMs, each with two to three emission scenarios are selected for investigation. A list of these models including their origin and associated scenarios is provided in Table 3.1.

Table 3.1 List of AOGCM models and emission scenarios used

GCM models	Sponsors, Country	Emission Scenarios	Atmospheric Resolution	
			Lat	Long
CGCM3T47, 2005	Canadian Centre for Climate Modelling and Analysis, Canada	A1B, B1, A2	3.75°	3.75°
CGCM3T63, 2005		A1B, B1,	2.81°	2.81°

		A2		
CSIROMK3.5, 2001	Commonwealth Scientific and Industrial Research Organization (CSIRO) Atmospheric Research, Australia	B1, A2	1.875°	1.875°
GISSAOM, 2004	National Aeronautics and Space Administration (NASA)/ Goddard Institute for Space Studies (GISS), USA	A1B, B1	3°	4°
MIROC3.2HIRES, 2004	Centre for Climate System Research (University of Tokyo), National Institute for Environmental Studies, and Frontier Research Centre for Global Change (JAMSTEC), Japan	A1B, B1	1.125°	1.125°
MIROC3.2MEDRES, 2004		A1B, B1, A2	2.8°	2.8°

### 3.2 Weather Generator

A weather generator model, one kind of downscaling technique, is employed to address the deficiencies (i.e. coarse spatial and temporal resolution) of global climate models for use at local scales. It stochastically simulates climate information for an area by combining both, local and global weather data. The local data are used to address the fine spatial and temporal scale issues needed for impact studies by including historically observed data obtained from stations in and around the study area. The global data provide the general direction of change of the climate within the region of interest by including outputs obtained from global climate models.

The principle component analysis integrated stochastic weather generator (KnnCADV3) is used in this study to produce synthetic data sets. The model is based on K-Nearest Neighbour (K-NN) algorithm developed by Sharif and Burn (2006). Recently Eum et al. (2009) revised the weather generator model of Sharif and Burn (2006) by adding the principal component analysis, which provides reduction in computational requirements and allows user to include more variables for an improved selection of nearest neighbours. The weather generator model operates by generating weather for a new day for a station of interest. This has been done by extracting all days with similar characteristics, known as nearest neighbours, from the historic record from which a single is selected according to a defined set of rules. The model also includes a perturbation mechanism which allows newly generated values to be outside of the observed

range. The data sets produced in this way take into account natural variability when predicting the effects of climate change.

The steps of the WG-PCA with  $p$  variables and  $q$  stations are as follows (Eum et al, 2009):

1) Regional means,  $\bar{X}_t$ , of  $p$  variables for all  $q$  stations are calculated for each day of the observed data:

$$\bar{X}_t = [\bar{x}_{1,t}, \bar{x}_{2,t}, \dots, \bar{x}_{p,t}] \quad \forall t = \{1, 2, \dots, T\} \quad (3.1)$$

$$\text{where } \bar{x}_{i,t} = \frac{1}{q} \sum_{j=1}^q x_{i,t}^j \quad \forall i = \{1, 2, \dots, p\} \quad (3.2)$$

2) Potential neighbours,  $L$  days long where  $L = (w+1) \times (N-1)$  for each of  $p$  individual variables with  $N$  years of historical record, and a temporal window of size ( $w$ ), are selected by the user of the weather generator. The days within the given window are all potential neighbours to the feature vector.  $N$  data which correspond to the current day are deleted from the potential neighbours so the value of the current day is not repeated (Eum et al, 2009).

3) Regional means of the potential neighbours are calculated for each day at all  $q$  stations.

4) A covariance matrix,  $C_t$  of size  $L \times p$  is computed for day  $t$ .

5) The first time step value is randomly selected for each of  $p$  variables from all current day values in the historical record.

6) (a) From the covariance matrix, ( $C_t$ ) the eigenvector and eigenvalue are calculated. (b) Selection of the eigenvector corresponding to the eigenvalue which represents the highest fraction of variance in the  $p$  variables. (c) The first principle component is calculated from Equations (3.3) and (3.4) using the eigenvector,  $E$ , found in (b).  $PC_t$  is the value of the current day and  $PC_k$  is the nearest neighbour transferred by the eigenvector in (b).

$$PC_t = \bar{X}_t E \quad (3.3)$$

$$PC_k = \bar{X}_k E \quad (3.4)$$

(d) The Mahalanobis distance is calculated with Equation (3.5) from the one dimensional matrix calculated by the above equations.

$$d_k = \sqrt{(PC_t - PC_k)^2 / \text{Var}(PC)} \quad \forall k = \{1, 2, \dots, k\} \quad (3.5)$$

where the variance of the first principle component is  $\text{Var}(PC)$  for all  $K$  nearest neighbours (Eum et al, 2009).

7) The number of nearest neighbours,  $K$ , out of  $L$  potential values is selected using  $K = \sqrt{L}$ .

8) The Mahalanobis distance  $d_k$  is put in order of smallest to largest, and the first  $K$  neighbours in the sorted list are selected (the  $K$  nearest neighbours). A discrete probability distribution is used which weights closer neighbours highest in order to resample out of the set of  $K$  neighbours. The weights,  $w$ , are calculated for each  $k$  neighbour as:

$$w_k = \frac{1/k}{\sum_{i=1}^k 1/i} \quad \forall k = \{1, 2, \dots, k\} \quad (3.6)$$

Cumulative probabilities,  $p_j$ , are given by:

$$p_j = \sum_{i=1}^j w_i \quad (3.7)$$

9) A random number  $u(0,1)$  is generated and compared to the cumulative probability calculated above in order to select the current day's nearest neighbour. If  $p_1 < u < p_k$ , then day  $j$  for which  $u$  is closest to  $p_j$  is selected. However, if  $u < p_1$ , then the day corresponding to  $d_1$  is chosen. If  $u = p_k$ , then the day which corresponds to day  $d_k$  is selected. Upon selecting the nearest neighbour, the K-NN algorithm chooses the weather of the selected day for all stations in order to preserve spatial correlation in the data (Eum et al, 2009).

10) In order to generate values outside the observed range, perturbation is used. A bandwidth is determined using:

$$\lambda = 1.06k^{1/5} \quad (3.8)$$

Perturbation is performed next, using:

$$y_{i,t}^j = x_{i,t}^j + \lambda \sigma_i^j z_t \quad (3.9)$$

where  $x_{i,t}^j$  is the weather variable obtained in step 9,  $y_{i,t}^j$  is the value of that variable obtained after perturbation,  $z_t$  is a random variable which is normally distributed (zero mean, unit variance) for day  $t$ . Negative values are prevented from being produced for precipitation by employing a largest acceptable bandwidth. If again a negative value is returned, a new value for  $z_t$  is generated (Sharif and Burn, 2006).

### 3.3 Hydrological Model

This study uses HEC-HMS to carry out hydrological simulations in a continuous mode. HEC-HMS is a computational modeling system developed by the Hydrologic Engineering Center (HEC) of the U.S. Army Corps of Engineers (USACE) in Davis, California. HEC-HMS is designed to simulate the precipitation-runoff process of watershed systems. Precipitation, air temperature, and estimated potential evapotranspiration are used as input data for HEC-HMS model. Additionally, soil information and land use data are required for estimating initial parameter sets for the model.

#### 3.3.1 Model Structure

Figure 3.1 represents the overall structure of the continuous hydrologic model. Each box in the figure represents a module that mathematically represents a physical processes functioning in the basin. Precipitation and maximum and minimum air temperature data obtained from the weather generator are used as inputs to a snow module, where adjustments are made to account for both solid and liquid precipitation. The output of the snow module is adjusted precipitation, used for computation of losses. The losses module represents the movement of moisture through various conceptual reservoirs within a catchment, such as canopy, surface, soil, and ground water. One of the outputs of the losses module is evapotranspiration, or moisture that evaporates from the canopy, surface depressions, and/or the soil. Baseflow (or lateral flow being returned to the stream from ground water), surface excess (the portion of the flow that does not infiltrate into the soil), and ground water recharge (the flow that enters deep aquifers and does not return to the stream) are other outputs from the losses module. The surface excess is converted to direct runoff by a unit hydrograph method. In the following the modules are described briefly:

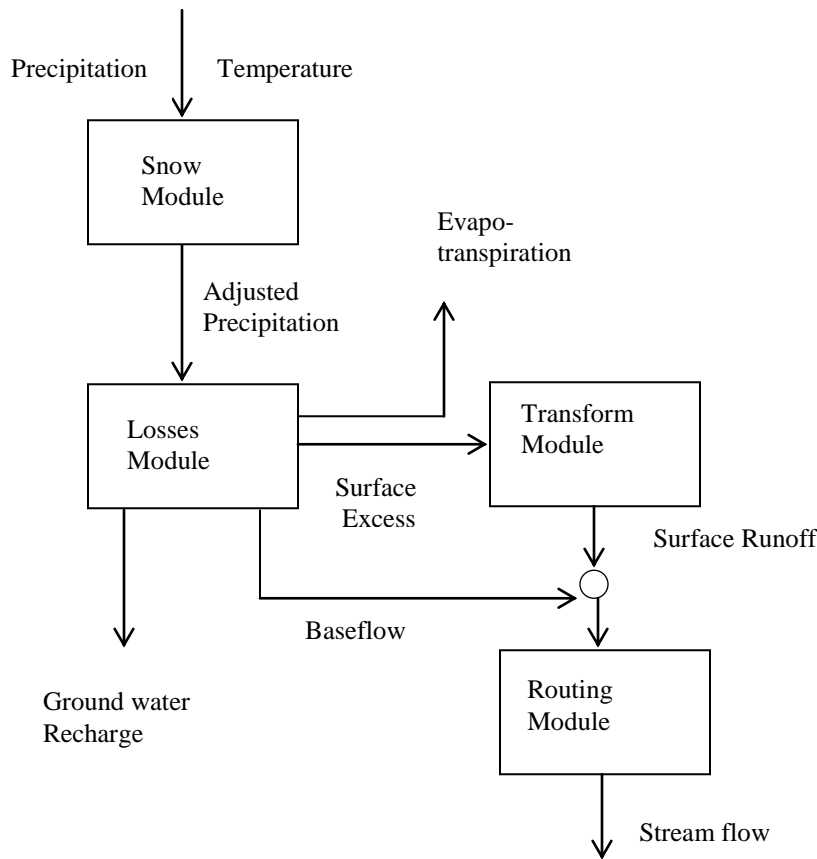


Figure 3.1 Continuous hydrologic model structure

### 3.3.2 Snow Module

In snow module degree day and threshold air temperature methods were used to estimate the snowmelt and snow accumulation. The precipitation and temperature data is integrated into the snow module to separate the solid (snow) and liquid (rainfall) forms of precipitation. The output of the snow module is adjusted precipitation.

The following sets of equations are used in this process. The measured amount of precipitation (mm/day) is categorized as rain  $R_i$  and snow  $S_i$  by the following equations:

$$\left. \begin{array}{l} S_i = P_i \\ R_i = 0 \end{array} \right\}, T_i < T_{\min} \quad (3.10)$$

$$\left. \begin{array}{l} S_i = P_i \cdot \left[ \frac{T_{\max} - T_i}{T_{\max} + T_i} \right] \\ R_i = P_i - S_i \end{array} \right\}, T_{\min} < T_i < T_{\max} \quad (3.11)$$

$$\left. \begin{array}{l} S_i = 0 \\ R_i = P_i \end{array} \right\}, T_i > T_{\max} \quad (3.12)$$

where  $i = 1, 2, 3, \dots, n$ : represents number of days with precipitation;  $T_{\min}$  and  $T_{\max}$  refer to the minimum and maximum temperature for snowfall and snowmelt, respectively.

The daily amount of snow melt is calculated as:

$$M_i = MR \cdot (T_i - T_c) \quad (3.13)$$

where  $MR$  represents a parameter for melt rate (mm<sup>0</sup>/C/day) set to 4.0 and  $T_c$  is a critical parameter for melt and is set to zero.

Adjusted precipitation is calculated from previously obtained snow-accumulation as:

$$S_i = S_i + S_{i-1} \quad (3.14)$$

If snowmelt occurs (i.e., if  $M_i > 0$ ) and if the accumulated snowmelt,  $S_i$ , is greater than the melt rate,  $M_i$ , ( $S_i > M_i$ ), then only a portion of the accumulated snow melts as:

$$S_i = S_i - M_i \quad (3.15)$$

On the other hand, if all accumulated snow melts, the adjusted precipitation becomes:

$$P_a = R_i + M_i \quad (3.16)$$

Lastly, if no snowmelt occurs, the adjusted precipitation takes on simply the value of rainfall as:

$$P_a = R_i \quad (3.17)$$

The adjusted precipitation is then used as input to the losses module.

### 3.3.3 Losses Module

The losses module incorporated within the HEC-HMS is called SMA (Soil Moisture Accounting). The module based on Precipitation-Runoff modeling System, PRMS (Leavesly and Stannard, 1995) was designed to compute runoff discharge on a continuous time basis. Conceptually, the SMA algorithm divides the potential path of rainfall in the watershed into five zones, as shown in Figure 3.2. The losses module uses a series of conceptual reservoirs to represent the storage and movement of water in each sub-catchment of the basin: (i) canopy interception, (ii) surface interception, (iii) soil profile, and (iv) a number of ground water layers (only two shown in Figure 3.2). The inflow and outflow rates between the reservoirs regulate the amount of water stored in each conceptual reservoir. These include evapotranspiration, infiltration, percolation, surface runoff and ground water flow. A more detailed description of the losses module can be obtained from Prodanovic and Simonovic (2006). The mathematical equations for the Soil Moisture Algorithm are well documented and can be found in Bennett (1998).

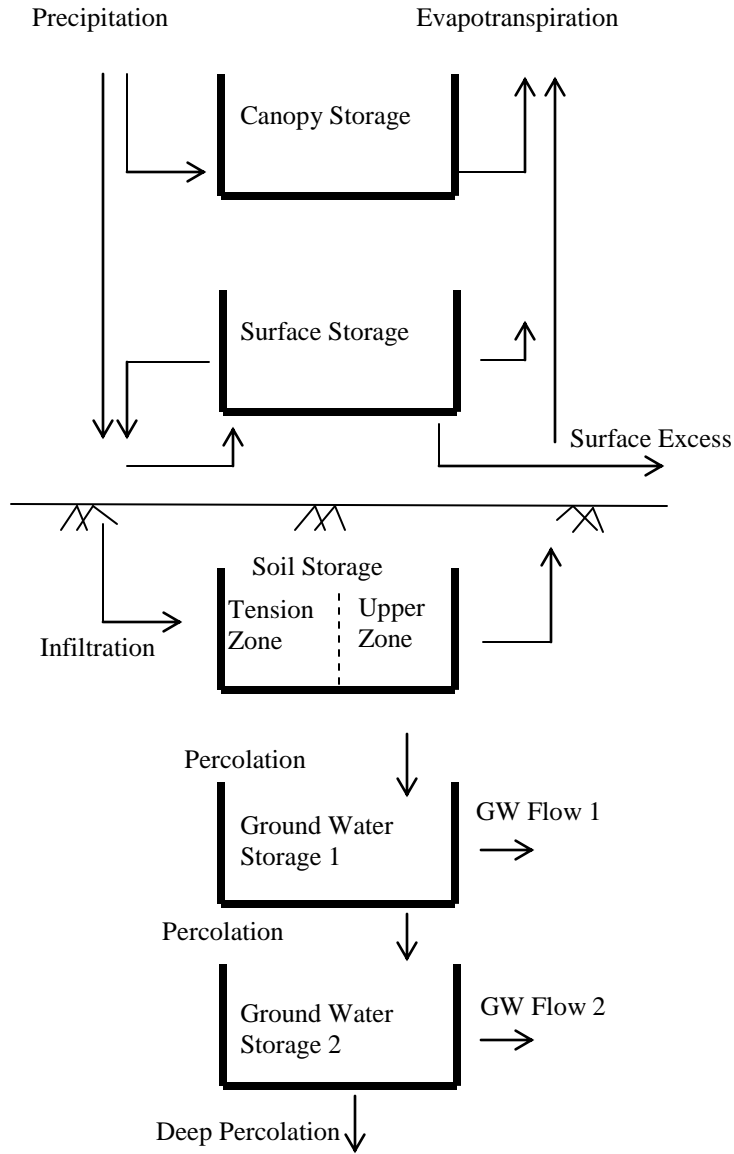


Figure 3.2 Soil moisture accounting losses module

### 3.3.4 Transform and Routing Modules

Clark's method (USACE, 2006) is used to convert surface excess into direct runoff. Similarly, the Modified Puls (USACE, 2006) method is used for routing flow in river reaches and the

reservoirs. A series of linear reservoirs is used to transform lateral ground water flow into the baseflow.

### 3.4 Statistical Analysis

In this study the peaks-over-threshold (POT) approach is chosen for flood frequency analysis. The statistical procedure associated with frequency analysis focuses on outlining an appropriate form to model, the underlying distribution of flood data, and then estimating the parameters of this distribution.

This study uses the method of L-moments to estimate parameters of a distribution. L-moments method introduced by Hosking (1990) is used because it is almost free of bias, easy to use and generally unaffected by outliers. L-moments are analogous to conventional moments defined as linear combinations of the probability weighted moments (PWMs) introduced by Greenwood et al. (1979). Theoretical formula in terms of the basic population quantities can be obtained from Hosking and Wallis (1997). Necessary relationships for the calculation of these statistics from the sample data can be obtained from Das (2010, p. 25).

#### 3.4.1 POT Modelling:

A peak over threshold series is formed by replacing the continuous hydrograph of flows by a series of randomly spaced spikes on the time axis. The series generally consists of well-defined flood peaks above a specified threshold ( $q_0$ ). In a POT model, such a series is fitted with a continuous probability distribution. The flood events are modelled by a discrete probability distribution, such as Poisson distribution, and the model is of the form:

$$1 - F(Q_T / Q_T > q_0) = \frac{1}{\lambda T} \quad (3.18)$$

where  $F( )$  is the cumulative frequency distribution of flood magnitude,  $Q > q_0$ .  $\lambda$  is the number of peaks per year included in the POT series. According to Cunnane (1989, p. 3), the POT model is statistically more efficient than the Annual Maximum (AM) model when  $\lambda > 1.65$ .

The generalized Pareto distribution (GPD), of which the exponential distribution (Cunnane, 1973; 1979) is a special case, with Poisson arrival rate has been the most popular model for POT series analysis (Wang, 1991; Rosbjerg et al., 1992). This follows from the result shown by Pickands (1975) that the generalized Pareto distribution arises as a limiting form for the distribution of independent exceedances over a high threshold. In this study the GPD with Poisson arrival rate is used for POT analysis.

### 3.4.2 Generalized Pareto Distribution (GPD)

This is a three parameter distribution and the distribution function is

$$F(q) = P(Q < q / q > q_0) = 1 - \left[ 1 - \frac{k}{\beta}(q - q_0) \right]^{\frac{1}{k}} \quad (3.19)$$

where  $q_0$  is the threshold  $\beta$  is a scale parameter and  $k$  is a shape parameter.

When  $k=0$ , this is reduced to exponential distribution of the form

$$F(q) = 1 - \exp\left[-\frac{1}{\beta}(q - q_0)\right] \quad (3.20)$$

The inverse form of the GPD is

$$q(F) = q_0 + \frac{\beta}{k} \left[ 1 - (1 - F)^k \right], k \neq 0 \quad (3.21)$$

$$q(F) = q_0 - \beta \ln[1 - F], k = 0 \quad (3.22)$$

The estimation of the parameters can be done in either of two distinct ways from a record of  $N$  years.

- a) Fix  $q_0$  a priori and abstract from the record of flows every peak value exceeding  $q_0$ . Let there be  $M$  of them
- b) An alternative to fix  $\lambda$  a priori. This determines  $M = \lambda N$  the required sample size. The largest  $M$  peaks are then extracted from the record and both  $q_0$  and  $\beta$  and  $k$  are estimated from a sample of data.

The estimation of the parameters using L-moments are as follows:

For case (a) the two parameters  $\beta$  and  $k$  are given by (Hosking and Wallis, 1997)

$$k = (l_1 - q_0) / l_2 - 2 \quad (3.23)$$

$$\beta = (1 + k)(l_1 - q_0) \quad (3.24)$$

For case (b), the three parameters are given by (Hosking and Wallis, 1997)

$$k = (l_1 - 3t_3) / (1 + t_3) \quad (3.25)$$

$$\beta = (1 + k)(2 + k)l_2 \quad (3.26)$$

$$q_0 = l_1 - (2 + k)l_2 \quad (3.27)$$

where  $l_1$  is 1<sup>st</sup> L-moment,  $l_2$  is 2<sup>nd</sup> L-moment and  $t_3$  is L-skewness

### 3.4.3 Selection of Peaks

Flood peaks can be obtained using different methods from a time series. The number of floods ( $M$ ) generally will be different to the number of years of record ( $N$ ), and will depend on the selected threshold discharge. The US Geological Survey (Dalrymple, 1960) recommended that

M should equal 3N. The UK Flood Studies Report (NERC, 1975) recommended that M should equal 3N to 5N.

A criterion for independence of successive peaks must also be applied in selecting events. Beard (1974) used a criterion that flood peaks should be separated by five days plus the natural logarithm of the square miles of drainage area, with the additional requirement that intermediate flows must drop to below 75% of the lower of the two separate flood peaks. The UK Flood Studies Report (NERC, 1975) used a criterion that flood peaks should be separated by three times the time to peak and that the flow should decrease between peaks to two thirds of the first peak. An excellent review on the selection of flood peaks is presented by Lang et al. (1999). In this study, the method proposed by Willems (2003, 2008) is used where two adjacent peaks are considered independent if:

- (i) the time between the two peaks is longer than the recession constant of the quick flow runoff components for the given basin;
- (ii) the minimum discharge between the two peaks is smaller than 37% of the peak discharge.

The POT values were extracted by applying the criteria mentioned above using the WETSPRO software, which has been developed by the Hydraulics Laboratory of K.U. Leuven in Belgium (Willems, 2003; 2008).

#### **3.4.4 Test of Suitability of GPD Distribution: L-Moment Ratio Diagrams**

The suitability of GPD probability distribution can be assessed with the help of L-moment ratio diagrams. The L-moment ratio diagrams are considered as a reliable diagnostic tool for identifying a probability distribution (Hosking and Wallis, 1997). The L-moment ratio diagram is a graph between L-kurtosis ( $\tau_4$ ) and L-skewness ( $\tau_3$ ). Usually a two-parameter distribution with a location and a scale parameter plots as a single point on such a diagram while a three parameter distribution with location, scale and shape plots as a line or curve on the diagram. Generally the distribution selection process involves plotting the sample L-moment ratios as a

scatter plot and comparing them with theoretical L-moment ratio points or curves of candidate distributions (Hosking and Wallis, 1997).

The GPD distribution is plotted as a line that corresponds to the varying shape parameters. The expressions for  $\tau_4$  are given as functions of  $\tau_3$  and are approximated as (Hosking and Wallis, 1997).

$$\tau_4 = 0.1224 + 0.30115\tau_3^2 + 0.95812\tau_3^4 - 0.57488\tau_3^6 + 0.19383\tau_3^8 \quad (3.28)$$

The Exponential distribution (a 2-parameter distribution) which is a special case of the GPD plots as a single point with a constant  $\tau_3$  value of 0.333, and a  $\tau_4$  value of 0.169. The L-moment ratio diagram has been successfully used in regional frequency analysis to select a distribution for a region (e.g. Das and Cunnane, 2011). In this context, a good number of POT series obtained from different AOGCMs allow the L-moment ratio diagram to be used.

### 3.4.5 Test of Poisson Process

The simplest Poisson model states that the occurrence of flood peaks in excess of a given threshold  $q_0$  conforms to a Poisson process, the number occurring in any year being a Poisson variate with parameter  $\lambda$ ,  $p(m \text{ peaks} > q_0 \text{ in a year}) = P_m = e^{-\lambda} \lambda^m / m!$  and that the flood peak magnitudes are identically, independently distributed (i.i.d) with distribution function  $F(Q \leq q / q \geq q_0)$  (Cunnane, 1979).

A test of the Poisson assumption can be conducted on a flow series of peaks exceeding  $q_0$ . The Poisson dispersion test introduced by (Cunnane, 1979) in POT flood frequency analysis provides the most powerful method for testing the adequacy of the fitted Poisson distribution. The statistic ( $D$ ) also known as Fisher dispersion statistic is based on the fact that the Poisson distribution, the mean and variance are equal.

The test statistic is as follows:

$$D = \frac{\sum_{i=1}^n (x_i - \bar{x})^2}{\bar{x}} \quad (3.29)$$

However it is shown by Cunnane (1979) in the context of POT analysis that while the Poisson assumption is a sufficient condition for flood magnitude-return period relationship, it is not a necessary one.

## **4 Case Study**

### **4.1 Description of the Watershed**

The methodologies described in the previous section are applied to the Upper Thames River basin (UTRb). The Upper Thames River basin has an area of 3,842 km<sup>2</sup> located between Lake Huron and Lake Erie in Southwestern Ontario. Majority of the river basin is covered with agricultural lands (80%), with forest cover and urban uses taking about 10% each. London is the major urban centre with a population of around 366,151 inhabitants, many of whom experience the effects of flooding as the Thames River runs directly through the City. The Thames River with a total length of 273 km has an average annual discharge of 35.9 m<sup>3</sup>/s. The UTRb receives approximately 1,000 mm of annual precipitation; however 60% of this is lost due to evaporation and evapotranspiration (Prodanovic and Simonovic, 2006). Figure 4.1 shows a schematic map of the Upper Thames River basin.

Flooding represents one of the major hydrologic hazards in the Upper Thames River basin. Flooding most frequently occurs after snowmelt, typically in early March; it also occurs as a result of summer storms usually taking place in July and August. In 1937, the City of London experienced a massive flooding event which eventually sparked the creation of the Upper Thames River Conservation Authority. Since then, three major water management reservoirs were created, namely Pittock, Wildwood, and Fanshawe (Prodanovic and Simonovic, 2007). Most recently such as in July 2000, April 2008 and December 2008, the Thames River has experienced several extreme flood events. Several weather stations are located throughout the basin to provide point measurements of climatic variables. Stations chosen for this study are listed in Table 4.1.

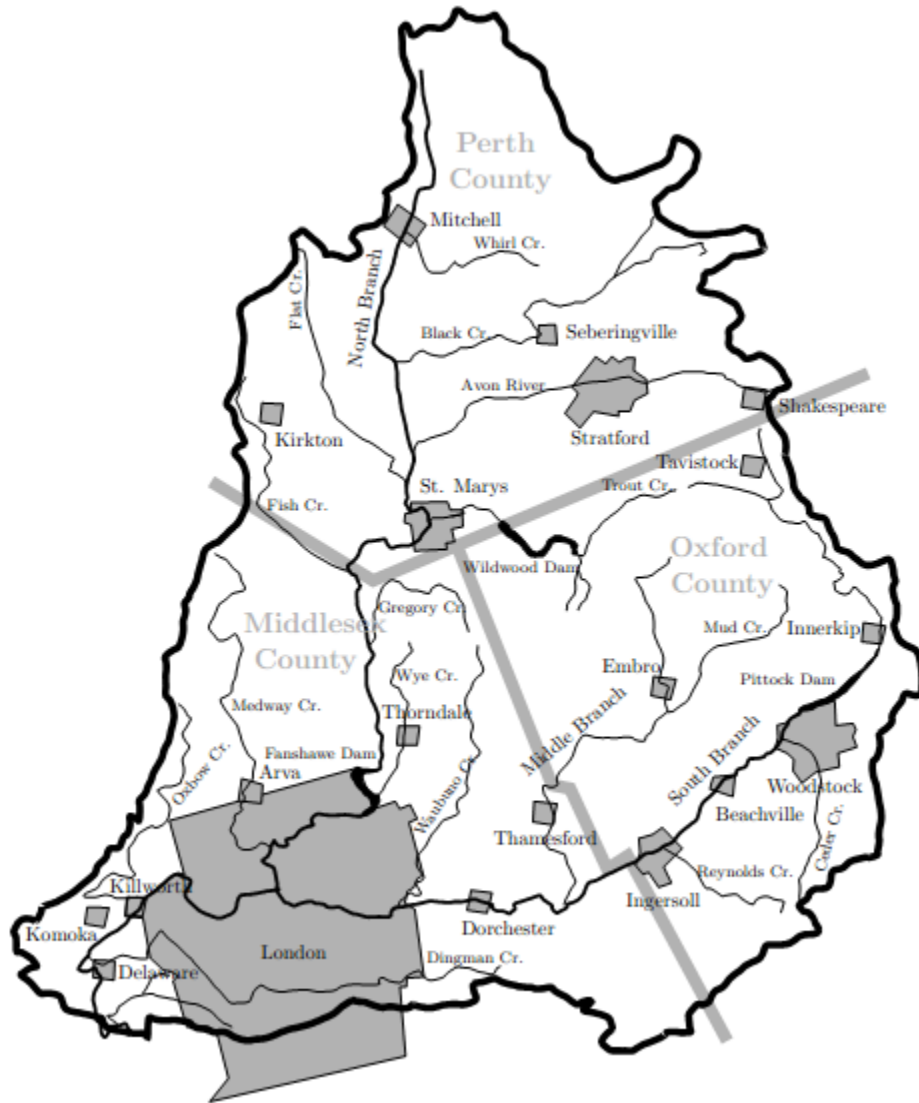


Figure 4.1 Map of the Upper Thames River basin

Table 4.1 Location of stations in the Upper Thames River basin

Station	Latitude(deg N)	Longitude(deg W)	Elevation(m)
Blyth	43.72	81.38	350.5
Brantford MOE	43.13	80.23	196
Chatham	42.38	82.2	198
Delhi CS	42.87	80.55	255.1
Dorchester	43	81.03	271.3
Embro	43.25	80.93	358.1
Exeter	43.35	81.5	262.1
Fergus	43.73	80.33	410
Foldens	43.02	80.78	328
Glen Allan	43.68	80.71	404
Hamilton A	43.17	79.93	238
Ilderton	43.05	81.43	266.7
London A	43.03	81.16	278
Petrolia Town	42.86	82.17	201.2
Ridgetown	42.45	81.88	210.3
Sarnia	43	82.32	191
Stratford	43.37	81	354
St. Thomas WPCP	42.78	81.21	209
Tillsonburg	42.86	80.72	270
Waterloo Wellington	43.46	80.38	317
Woodstock	43.14	80.77	282
Wroxeter	43.86	81.15	355

## **4.2 Hydrological Model Setup, Calibration and Validation**

The hydrologic model has been originally developed and applied to the Upper Thames River in the work by Cunderlik and Simonovic (2004, 2005). The hydrologic model consists of thirty three sub-basins, twenty one river reaches, and three reservoirs namely Wildwood, Fanshawe and Pittock. The schematic of the model is shown in Figure 4.2. Each sub-basin in Figure 4.2 is represented by rectangles and is provided with interpolated precipitation and maximum and minimum temperature data. The outputs of each sub basin are flow hydrographs joined by junctions (circles) where the flows are added together. River reaches represent the major rivers in the basin and are shown as thick lines connected between two junctions. The routing module is applied to each river reach, and thus acts as a passage of a flood wave as it moves through the river system. Reservoirs are depicted as triangles and the same routing rules are applied.

The hydrologic model applied to the Upper Thames River basin has been calibrated and verified with extensive sensitivity analyses (Cunderlik and Simonovic, 2004; 2005). The model is seasonal in nature with different parameters referring to the summer and winter seasons. The parameter sets for the summer and winter seasons are presented in Cunderlik and Simonovic (2004) and Prodanovic and Simonovic (2007). In this report no attempt has been made to recalibrate the model.



### 4.3 Data Source and Production of POT Series

The following steps are implemented to produce POT series for a stream gauge under climate change. Byron stream gauge, located in South-East of the Upper Thames River basin, is selected for this study.

1. Daily weather data (precipitation, maximum temperature and minimum temperature) for the period of 1979-2005 was obtained from Environment Canada ([http://www.climate.weatheroffice.gc.ca/climateData/canada\\_e.html](http://www.climate.weatheroffice.gc.ca/climateData/canada_e.html)) for each of the stations listed in Table 4.1. Stations were chosen based on the completeness and length of the observed data. The historic daily flow data for the Byron gauging station was obtained from Environment Canada (<http://www.wateroffice.ec.gc.ca>).
2. Climate data for each of the fifteen AOGCM's scenarios have been collected from the nearest grid points surrounding the Upper Thames River Basin. The Canadian Climate Change Scenarios Network (CCCSN) provides access to those AOGCM models and emissions scenarios. Data have been obtained for four time slices: 1961-1990, 2011-2040, 2041-2050 and 2071-2100. Seven variables were chosen: minimum temperature, maximum temperature, precipitation, specific humidity, northward wind component, southward wind component and mean sea level pressure.
3. Climate variables from the nearest grid points have been interpolated to provide a data set for each of the stations of interest. For the purpose of interpolation the inverse distance weighting (IDW) (for calculation see King et al., 2009) is used. This method is widely used, and recommended by the United States Army Corps of Engineers (USACE, 2000).
4. Calculation of change factors for future climate is performed. Using the AOGCM datasets for each station, monthly averages are computed for each variable for both the baseline (1960-1990) and the future time slices (2011-2040, 2041-2070 or 2071-2100).

For maximum temperature, minimum temperature, northward wind speed, eastward wind speed and mean sea level pressure, the monthly change factors are computed as the difference between the baseline and the future averages. For precipitation and humidity, the change factors are taken as the percent change between the baseline and the future averages. The change factors have been used to modify the historic datasets for each station gathered from Environment Canada. The historical daily data for humidity and precipitation are multiplied by the monthly change factors. For the rest of the variables, the change factors are added to modify the historical data.

5. Modified historic data sets, are used as input into the WG-PCA to produce a synthetic dataset. This study uses 22 stations for the period of 1979-2005 ( $N=27$ ) to simulate different rainfall scenarios. Employing the temporal window of 14 days ( $w=14$ ) and 27 years of historic data ( $N=27$ ), 390 days are considered as potential neighbors ( $L=(w+1) \times (N-1)=390$ ). Each case is simulated 25 times. Another scenario “baseline” (historical perturbed data) is developed to describe the climate that will continue to change as the consequence of already altered greenhouse gas concentrations in the atmosphere, ignoring any future change in greenhouse gas emissions.
6. The locations of 22 stations for climate data do not correspond to the locations of the sub-basins. The climatic data derived from the weather generator is therefore spatially interpolated in order to be used by the hydrologic model. The Inverse Distance Weighting Method (USACE, 2000) is used for interpolation. The interpolated synthetic data series of precipitation, maximum and minimum air temperature are fed into the calibrated hydrological model to get the simulated flow series for the four time horizons.
7. Peaks are extracted from the flow series for the Byron station at an average rate of three per year (i.e. the peak threshold is implicit), using the set of rules defined in Section 3.4.3. Thus 81 most extreme floods are selected for each of the flow series.

## 5 Results and Discussions

This section presents the results of the statistical procedures applied to the POT data series produced for Byron stream gauging station located at the Upper Thames River basin under changing climate conditions.

### 5.1 Peak Flows

POT series are obtained for each future time horizon (2020, 2050 and 2080) and for the baseline (1979-2005). A total of 375 POT series (15 AOGCMs x 25 model runs each) are derived for future climate projections (2020, 2050 and 2080). For baseline, 25 POT series are obtained by perturbing historical data 25 times using the weather generator. Figure 5.1 shows the Box-plots of peak discharges for each AOGCM for all the time horizons. Baseline is included in each future time horizon for the comparison. By 2020, Canadian climate models (CGCM3T47 and 63) under scenarios A1B, A2, B1, suggest a 7-16% (median) increase in peak discharge, whereas rest of the models propose a 4-16% (median) decrease compared to the baseline period. By 2050, climate models MICROC3HIRES and GISSAOM under scenarios A1B and B1, suggest a 1-8% (median) decrease in peak discharge, whereas rest of the AOGCMs propose an 8-28% (median) increase in peak discharge compared to the baseline period. The largest increase is projected by CSIROMK3.5\_A2. By 2080, climate models, MICROC3HIRES under scenarios A1B and B1 and CSIROMK3.5 under scenario B1 propose a 2-11% median decrease, whereas rest of the AOGCMs suggest a 2-44% (median) increase in peak discharge compared to the baseline period. The largest increase at 44% is projected by CGCM3T63\_A1B. The maximum discharge is projected by CGCM3T63\_A2, MICROC3MEDRES\_B1 and CGCM3T47\_A2, respectively for the 2020, 2050 and 2080 time horizon. This shows the variability of peaks projected by different climate models under different emission scenarios in different time horizons.

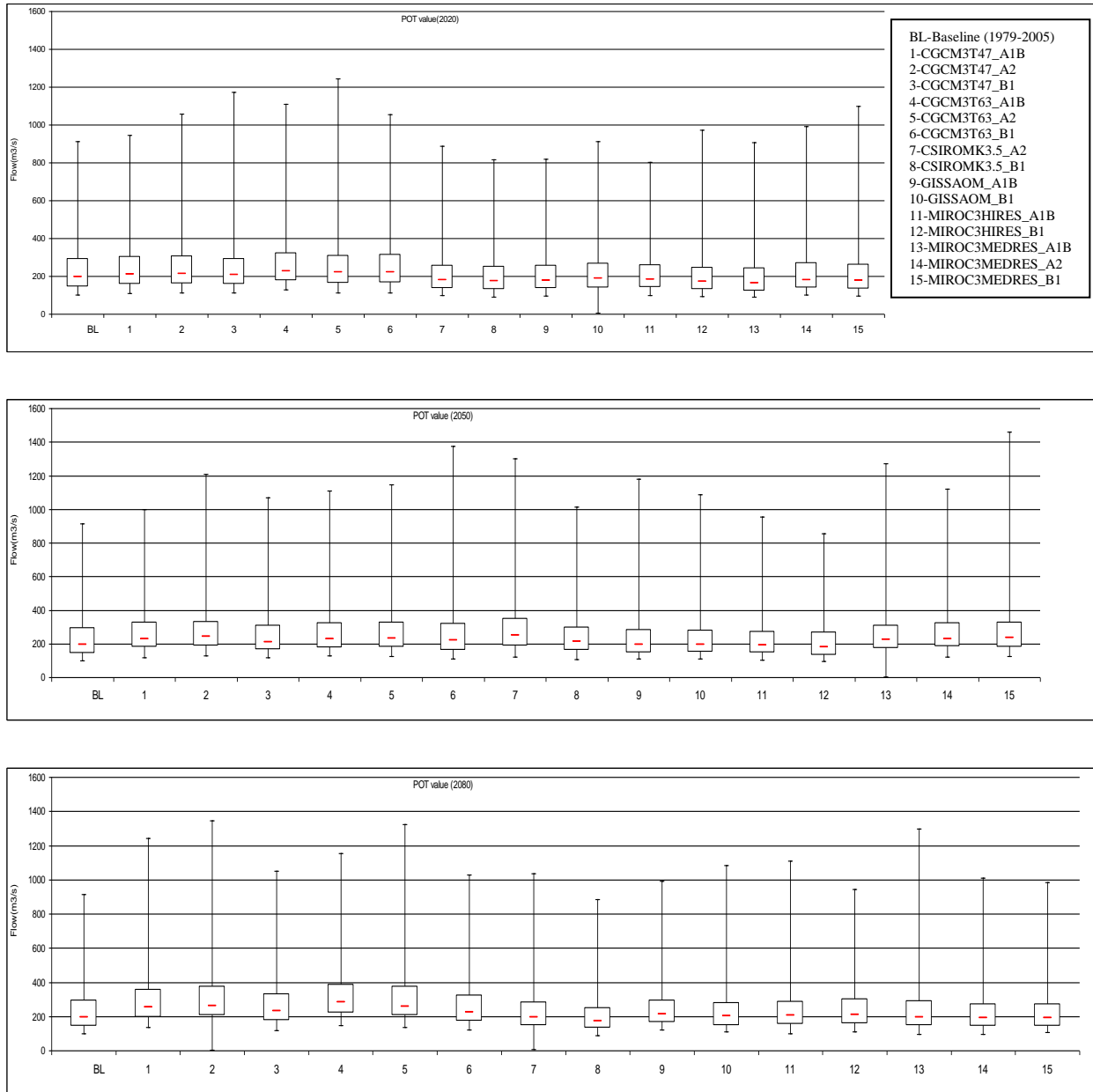


Figure 5.1 Box-plots of peak discharges for all AOGCMs considered in this study. Results are for the Byron gauging station in the Upper Thames River basin at the 2020, 2050 and 2080 time horizons. The baseline period (BL) is also included with each future time horizon.

## **5.2 Evaluation of POT Modelling**

This section presents the results related to POT modelling.

### **5.2.1 Suitability of GPD Distribution**

The L-moment ratio diagrams (LMR) were constructed for all four time horizons and they are displayed in Figure 5.2. The LMR for baseline is constructed with 25 data points, one for each model run. The LMRs for future time horizons are constructed with 375 data points (15 AOGCMs x 25 model runs each). The average of the data points is shown as square. The GPD is shown as a curve whereas the Exponential distribution which is a special case of GPD is shown as a single point (circle). Figure 5.2 shows except for baseline, the peaks follow the GPD distribution very well. The average data point is also very close on those cases to the population L-moments of an exponential distribution. This indicates that the two parameter GPD distribution is also capable of describing the data very well. Therefore either GPD or its special case Exponential distribution can be used to describe POT flood data for future climate.

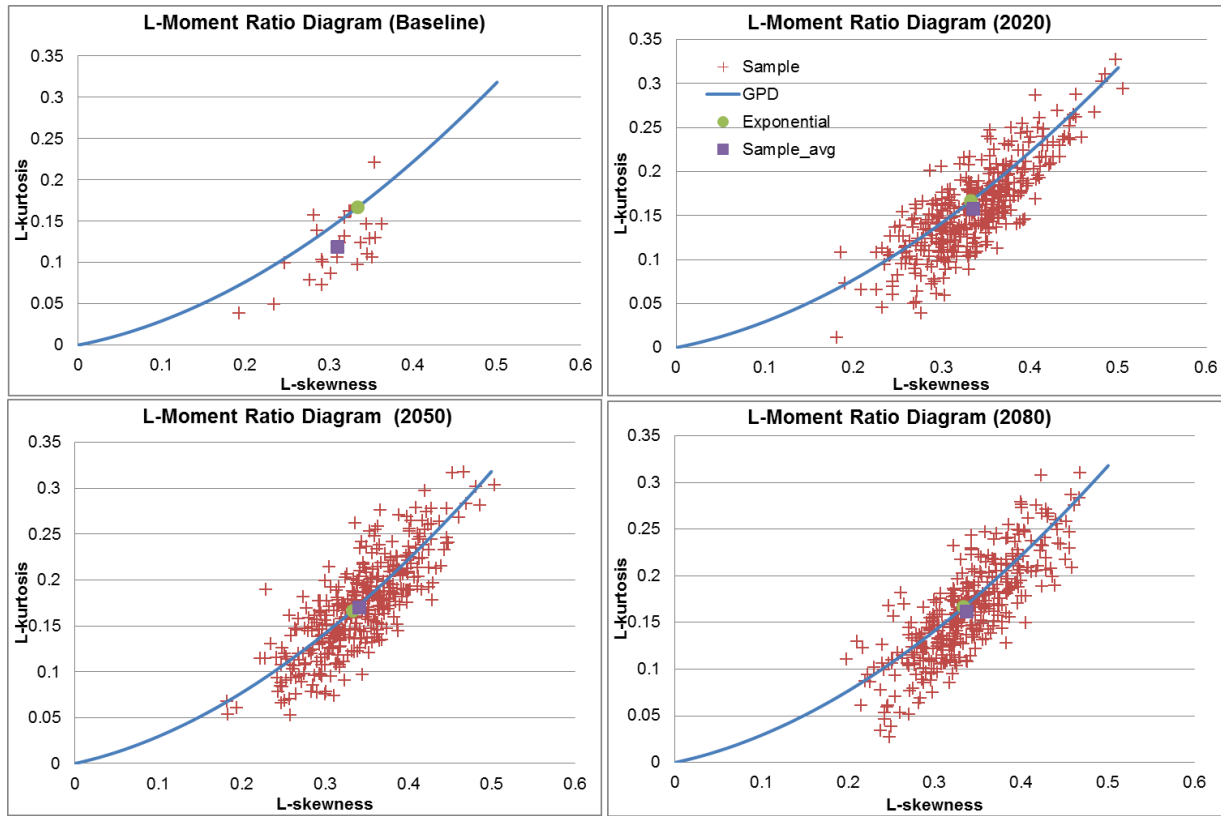


Figure 5.2 L-moment ratio diagrams for POT series obtained for all future climate projections, and for the baseline period (BL)

### 5.2.2 Poisson Process

Dispersion test described in Section 3.4.5 is used to test the Poisson process. The dispersion index,  $D$ , is calculated for POT series obtained for all the future time horizons. The test is evaluated at the 0.05 significance level, which means that it is expected that if the Poisson model is reasonable for the data, it is rejected in about 5% of cases. Table 5.1 summarizes the % of times out of  $x$  datasets (for BL,  $x = 25$ ; for future climate,  $x = 375$ ) that Poisson is rejected by the test. The  $D$  rejected Poisson about 50% of all cases suggesting that peaks derived in this study follow Poisson distribution in about 50% cases. It can be mentioned here that for obtaining a flood magnitude-return period relationship using a POT series, the Poisson assumption is not a necessary one (Cunnane, 1979).

Table 5.1 Percentage of rejections at the 5% significance level for the dispersion test

	Baseline	2020	2050	2080
Poisson	52%	42%	55%	47%

### 5.2.3 Shape Parameter Uncertainty

The value of the shape parameter and its precision is important in POT modelling using the GPD. Estimated shape parameter from a data series has a significant amount of uncertainty. Therefore an evaluation of the parameter for all data sets is needed, and is performed in this section. Figure 5.3 displays the boxplots for the shape parameter for all time horizons. This shows how the parameter values vary for each of the data sets in each time horizons. It is suggested that the upper and lower values indicated by the box i.e. containing the middle 50% of values, ought to give a good indication of the range of true values. For BL the range is between -0.09 and 0.1 (median value is .05), which indicates most of the cases the distribution is upper-bounded. For the future time horizons (no particular trend was observed among the three horizons) the ranges are between -0.1 and 0.1 with median value zero indicates a decreasing trend compared to BL. Thus overall results show that the future data can be described with GPD with shape parameter,  $k = 0$ , in other words with an Exponential distribution.

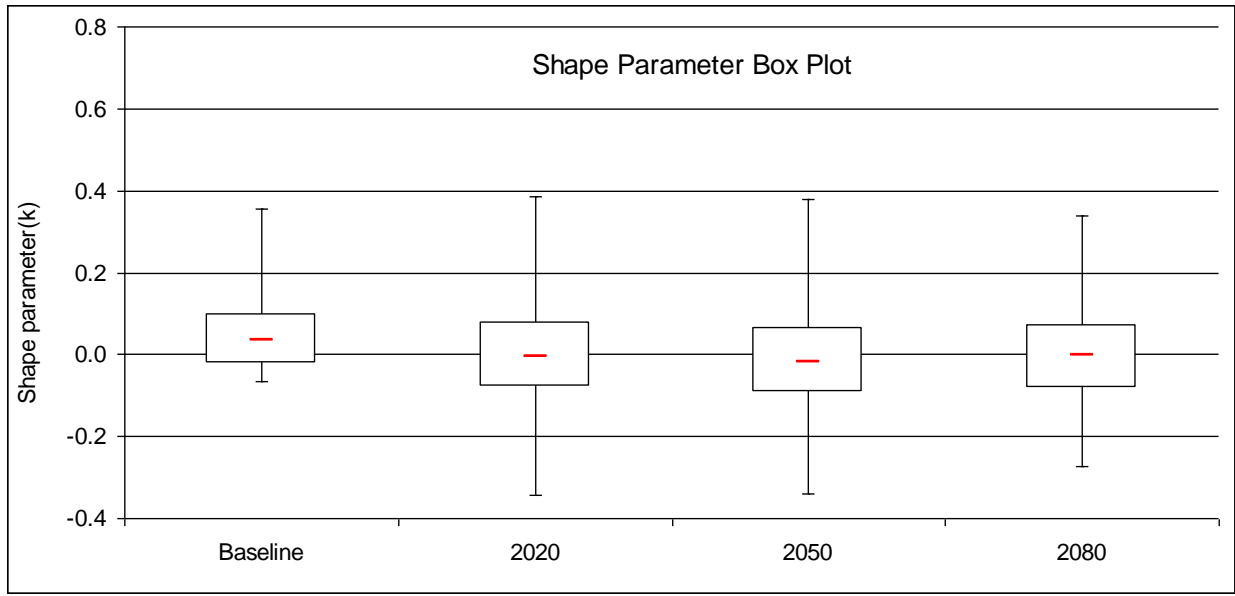


Figure 5.3 Box plots of shape parameter of GPD distribution at the four time horizons

### 5.3 Flood Magnitude - Return Period Relationship and Uncertainties

POT data derived from different AOGCMs are used to estimate Flood magnitude-Return period relationships (Q-T curves) for all time horizons. It is hoped that employing a good number of different AOGCM scenarios the many variations of climate change encompassing all uncertainties were taken into account, which give a wide variety of results to analyze. The T-year return period flood magnitudes for all climate model scenarios are produced using the GPD model.

Figure 5.4 to Figure 5.7 display the flood frequency curves (Q-T) for all the time horizons. The flood frequency curve derived from historic data is also shown for information only. The AOGCMs for the highest and the lowest frequency curves are also shown in the figure. For example, for 2020 the highest and lowest frequency curves are obtained from a model run derived from CGCM3T63-A2 and MICRO3MEDRES-A1B, respectively. It is found that the corresponding magnitudes for 100 (250)-year floods are respectively 1175(1626) and 391(478)  $\text{m}^3/\text{s}$ .

These indicate how the return values vary with the application of different AOGCMs, due to the assumptions made in each model.

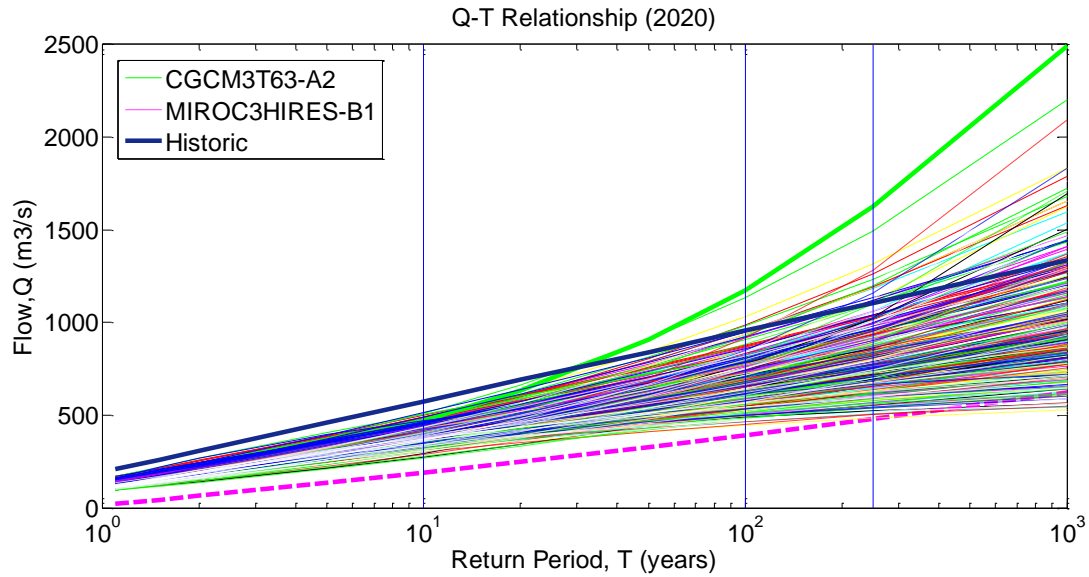


Figure 5.4 Simulated flood frequency results for climate data at time horizon 2020. Data from 375 scenarios (15 climate model scenarios x 25 model runs each) are used. Each line with a specific color represents a different AOGCM. The upper and lower bound frequency curves are obtained from scenario runs derived from CGCM3T63-A2 and MICRO3HIRES-B1, respectively.

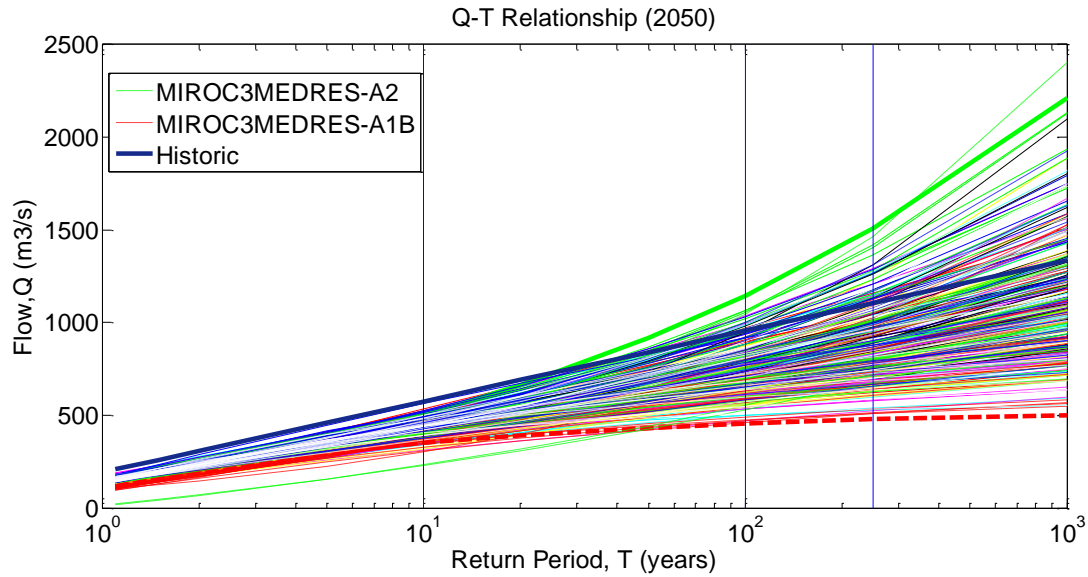


Figure 5.5 Simulated flood frequency results for climate data at time horizon 2050. Data from 375 scenarios (15 climate model scenarios x 25 model runs each) are used. Each line with a specific color represents a different AOGCM. The upper and lower bound frequency curves are obtained from scenario runs derived from MICRO3MEDRES-A2 and MICRO3MEDRES-A1B, respectively.

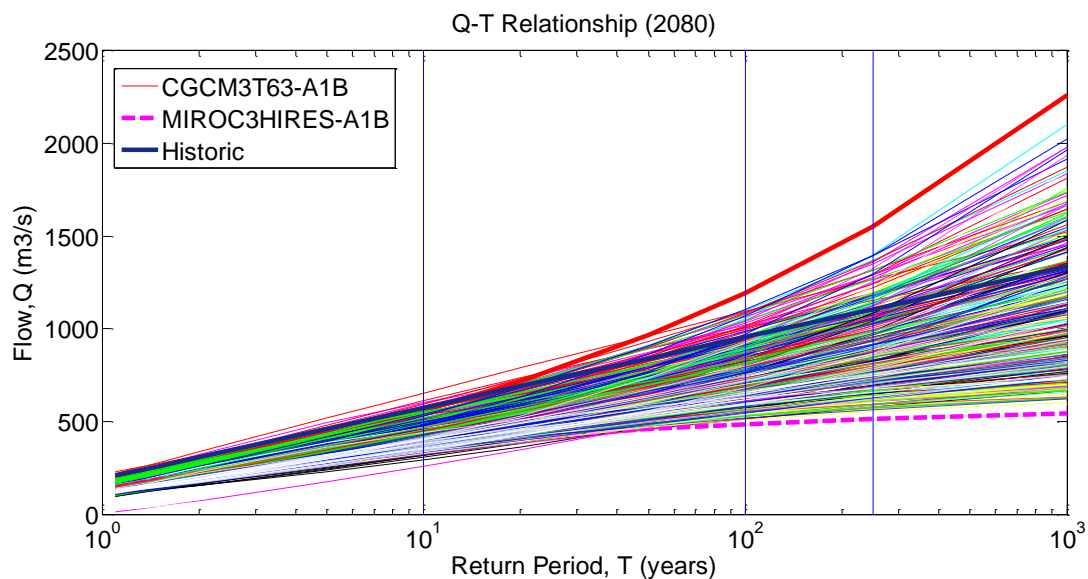


Figure 5.6 Simulated flood frequency results for climate data at time horizon 2080. Data from 375 scenarios (15 climate model scenarios x 25 model runs each) are used. Each line with a specific color represents a different AOGCM. The upper and lower bound frequency curves are

obtained from scenario runs derived from CGCM3T63-A2 and MICRO3MEDRES-A1B, respectively.

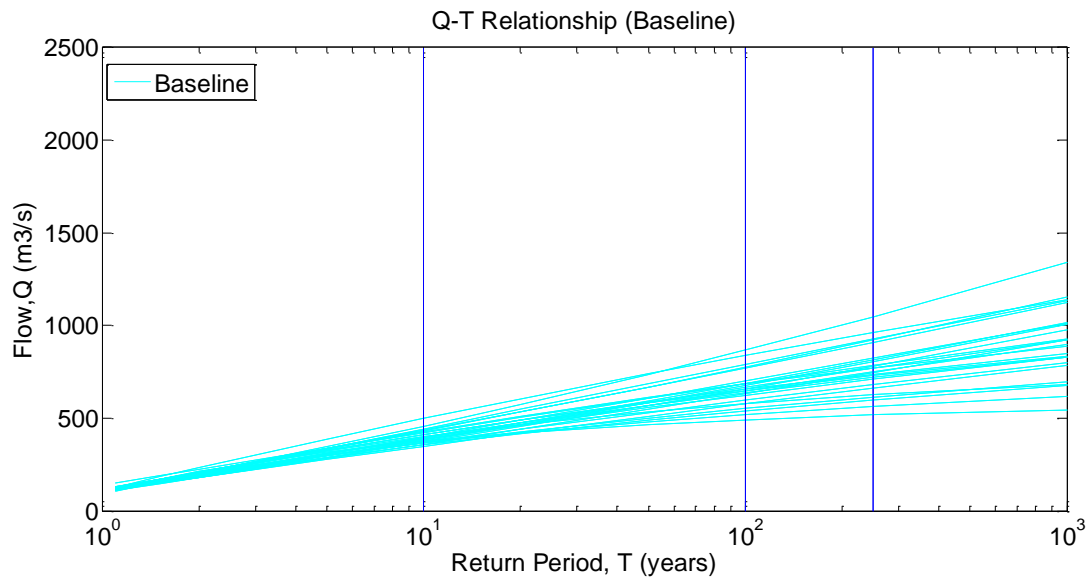


Figure 5.7 Simulated flood frequency results for climate data at baseline. Data from 25 runs produced a range of results.

The frequency curves for Canadian models (CGCM3T47 and 63) under emission scenarios A1B, A2 and B1 are grouped together to show how Canadian models performed in terms of Q-T relationship. They are displayed in Figures 5.8, 5.9 and 5.10 for the time horizon 2020, 2050 and 2080 respectively. These climate models are of particular interest because the study region is located in Canada. The upper and lower bound frequency curves for 2020 time horizon were obtained from scenario runs derived from CGCM3T63-A2 and CGCM3T63-B1, respectively. For 2050, they were from CGCM3T63-A2 and CGCM3T63-A1B, respectively, while for 2080 they were from CGCM3T63-A1B and CGCM3T47-B1, respectively.

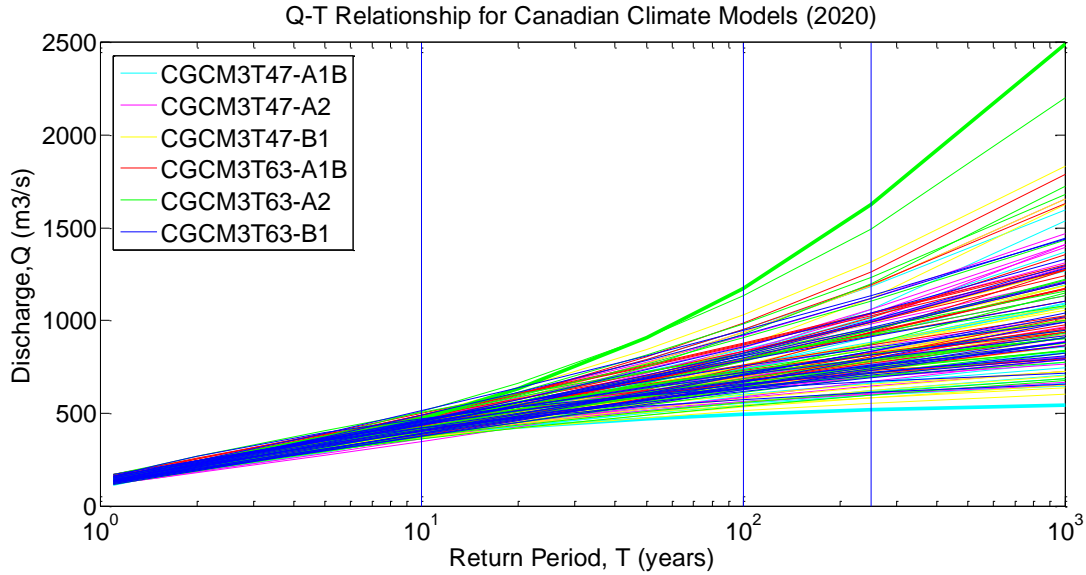


Figure 5.8 Simulated flood frequency results for climate data at time horizon 2020. Data from 150 scenarios (6 Canadian climate model scenarios x 25 model run each) are used. The upper and lower bound frequency curves are obtained from scenario runs derived from CGCM3T63-A2 and CGCM3T47-A1B, respectively.

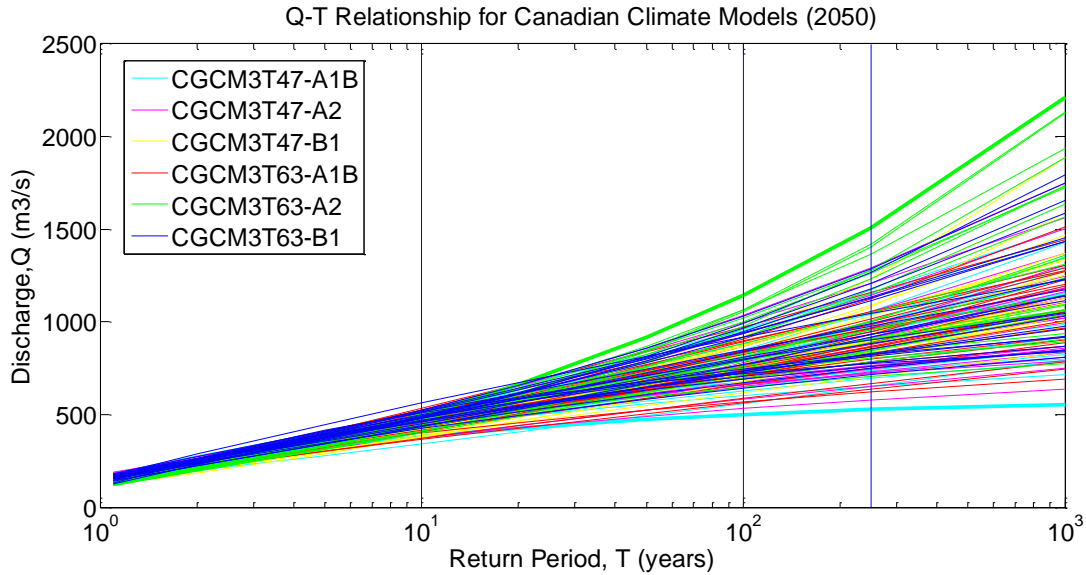


Figure 5.9 Simulated flood frequency results for climate data at time horizon 2050. Data from 150 scenarios (6 Canadian climate model scenarios x 25 model run each) are used. The upper and lower bound frequency curves are obtained from scenario runs derived from CGCM3T63-A2 and CGCM3T47-A1B, respectively.

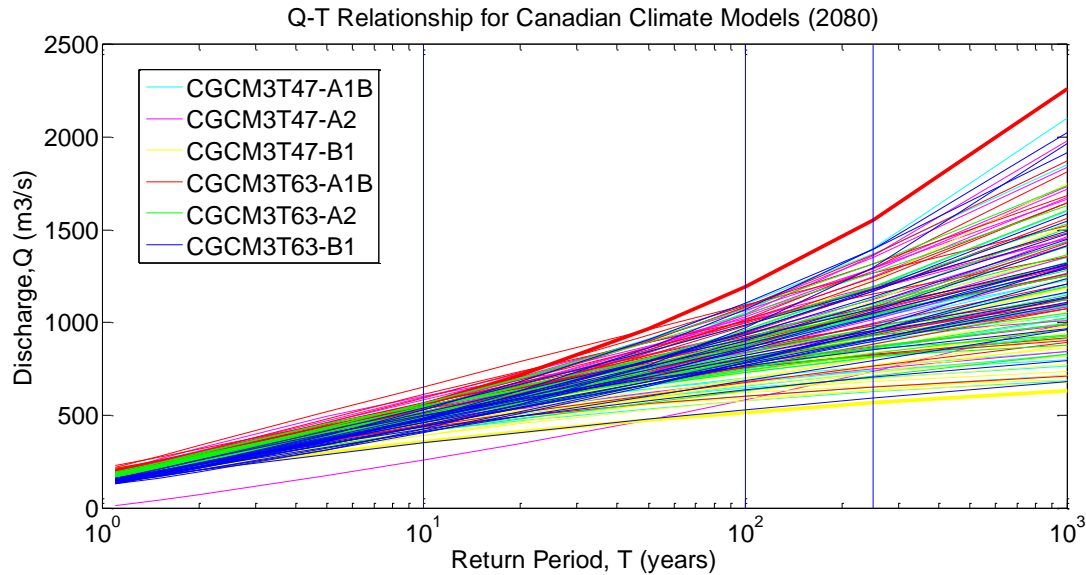


Figure 5.10 Simulated flood frequency results for climate data at time horizon 2080. Data from 150 scenarios (6 Canadian climate model scenarios x 25 model run each) are used. The upper and lower bound frequency curves are obtained from scenario runs derived from CGCM3T63-A1B and CGCM3T63-B1, respectively.

A large number of flow values (15 AOGCMs X 25 model runs each = 375 data series) obtained for different model scenarios for a particular return period can be assumed to be a good representation of flow variability under climate change and these can be used to establish an uncertainty measure. The simplest normal assumption or non-parametric assumption (e.g., Solaiman and Simonovic, 2011) can be employed to estimate an uncertainty bound. Non parametric based approach, normal kernel function, is used in this study to construct probability density functions (PDF). The PDFs allow the uncertainty of design flow to be better quantified. Figure 5.11 shows the PDFs of 100-year return period flood for each AOGCMs at time horizon 2050. The PDFs are constructed for each AOGCM using 25 model runs. The PDFs are different for different AOGCMs. A greater variance is observed for the climate models, CGCM3T63-A2 and MICRO3MEDRES-B1. The PDFs of floods at return periods,  $T = 10, 100$  and  $250$ , for the time horizons 2020, 2050 and 2080 are shown in Appendix A.

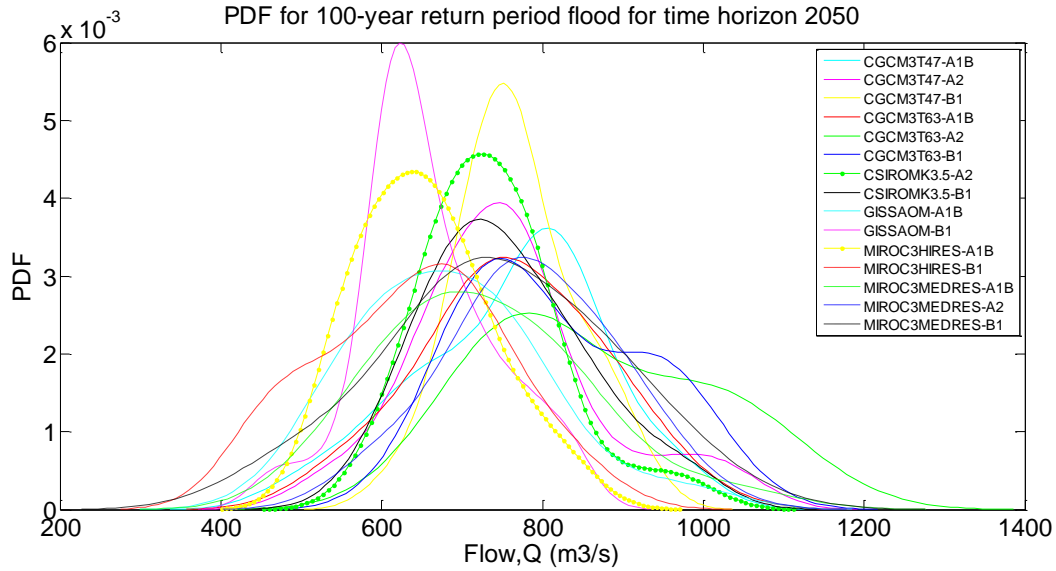


Figure 5.11 Probability density functions (PDFs) of 100-year return period flood for all AOGCMs at the time horizon 2050. Each PDF is constructed using 25 model runs.

Data from 15 climate models are employed to construct probability density plots for floods at return period,  $T = 10, 100$  and  $250$  for the four time horizons for comparison. The plots are displayed in Figures 5.12, 5.13 and 5.14. It is to be mentioned that the corresponding  $T$ -year floods based on historic data are  $574, 955$  and  $1107 \text{ m}^3/\text{s}$ , respectively. Results show that uncertainty increases with time, as PDFs become flatter. A greater variance of the design flood is also observed as PDFs become generally flatter with time. It is found that the average percentage changes of the 100-year flood magnitude between the future climate (2020, 2050 and 2080) and the baseline (1979-2005) are respectively 8, 12 and 12.3%. The corresponding percentage changes for the 250-year flood are respectively 19, 32 and 32.5%.

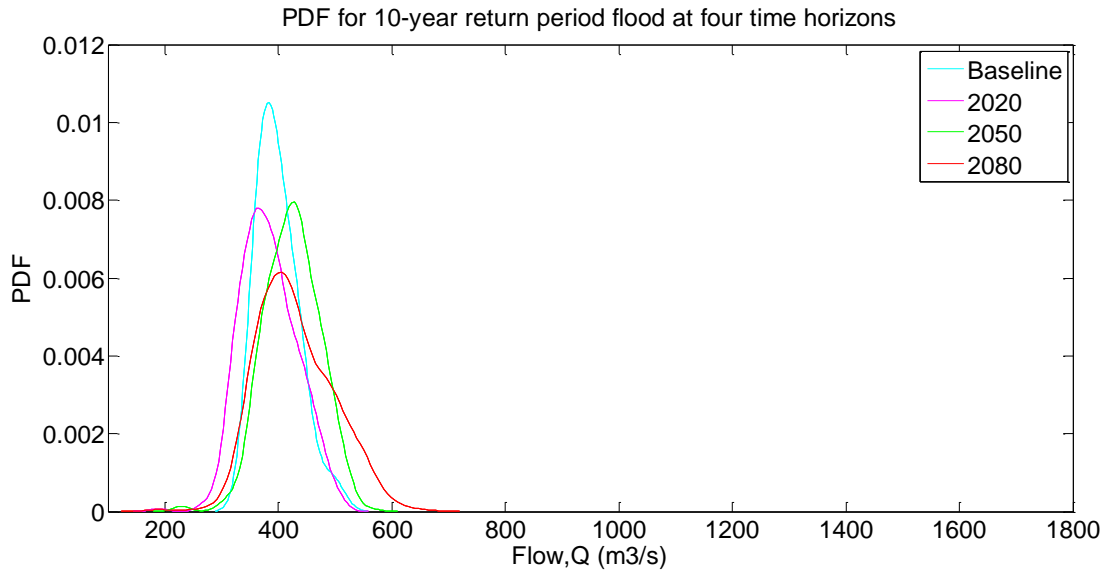


Figure 5.12 Probability density plots for 10-year return period flood for the four time horizons.

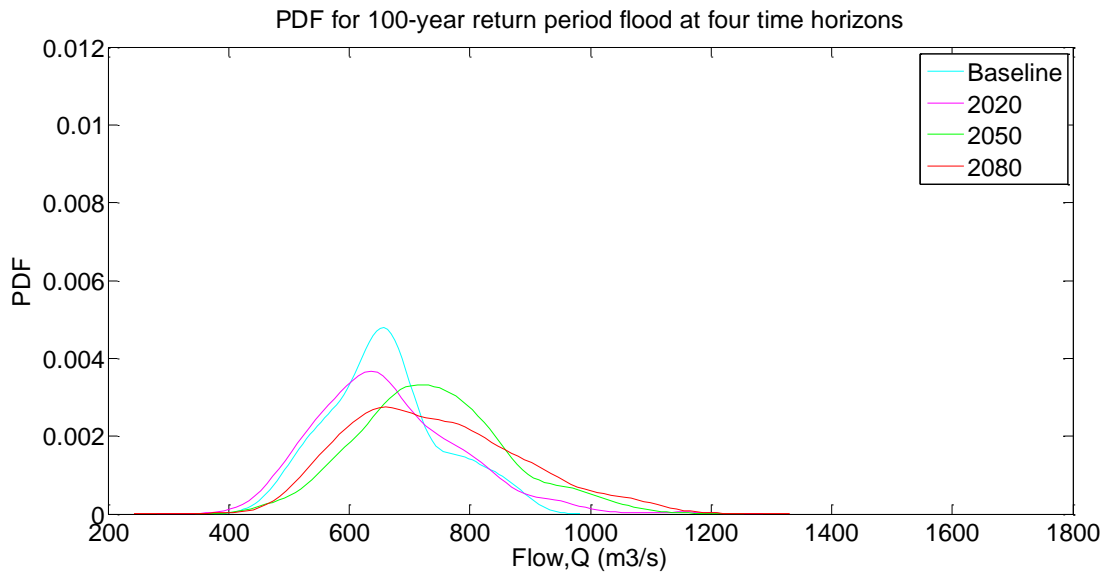


Figure 5.13 Probability density plots for 100-year return period flood for the four time horizons.

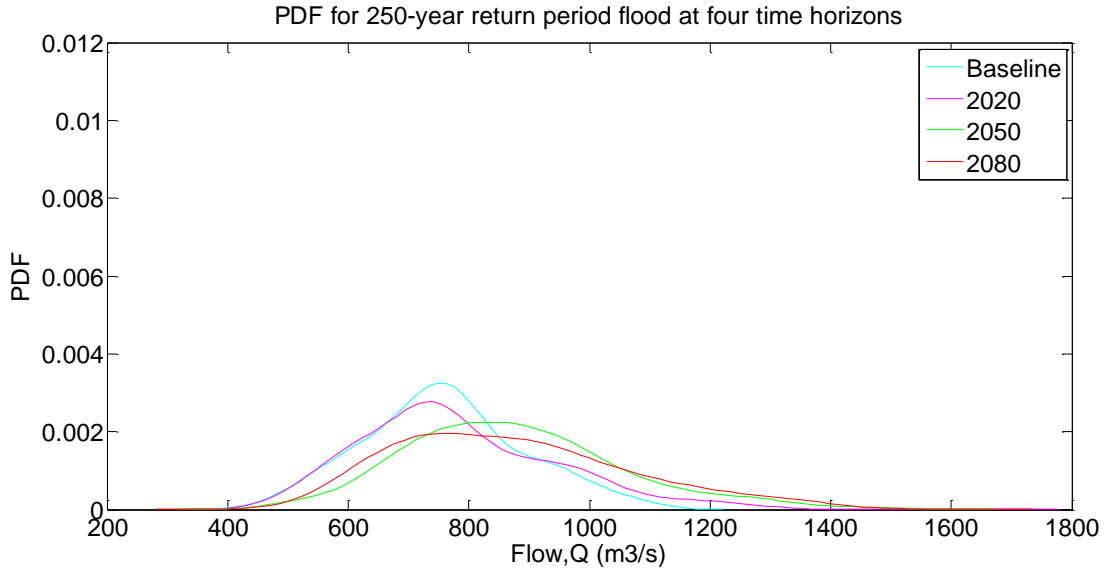


Figure 5.14 Probability density plots for 250-year return period flood for the four time horizons.

The information from the above figures, Figure 5.12, 5.13 and 5.14, are converted to cumulative distribution functions (CDFs). They are displayed in Figures 5.15, 5.16 and 5.17 for 10, 100 and 250-year return period flood, respectively.

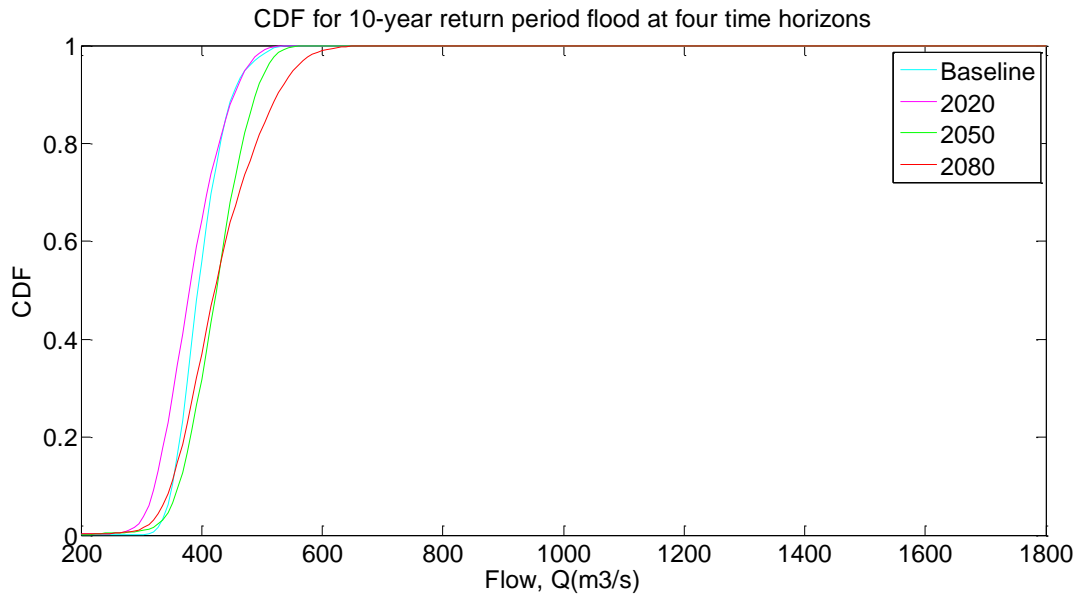


Figure 5.15 CDFs for 10-year return period flood for the four time horizons.

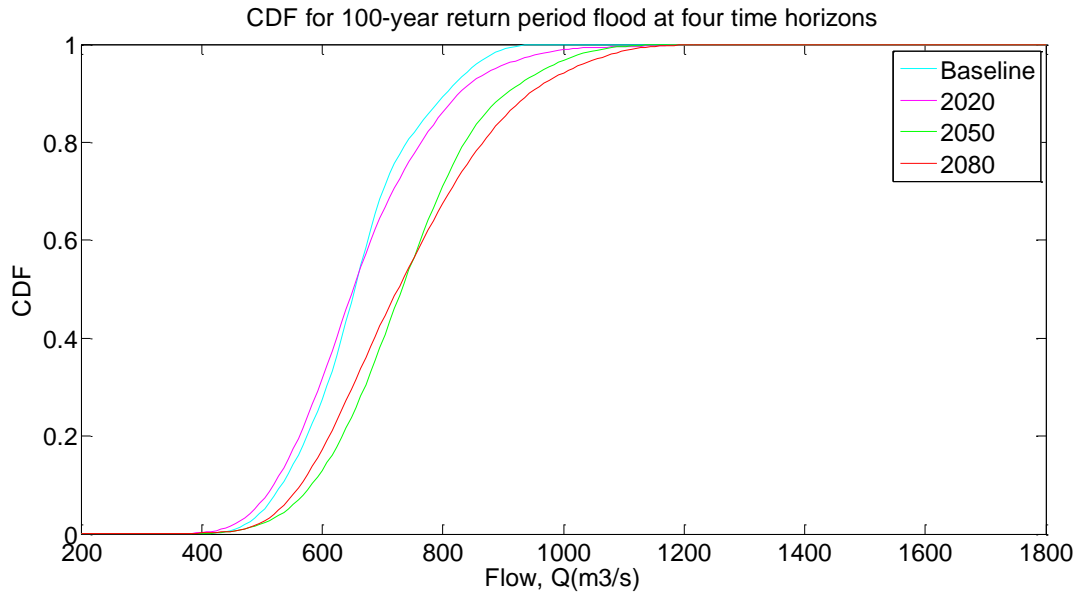


Figure 5.16 CDFs for 100-year return period flood for the four time horizons.

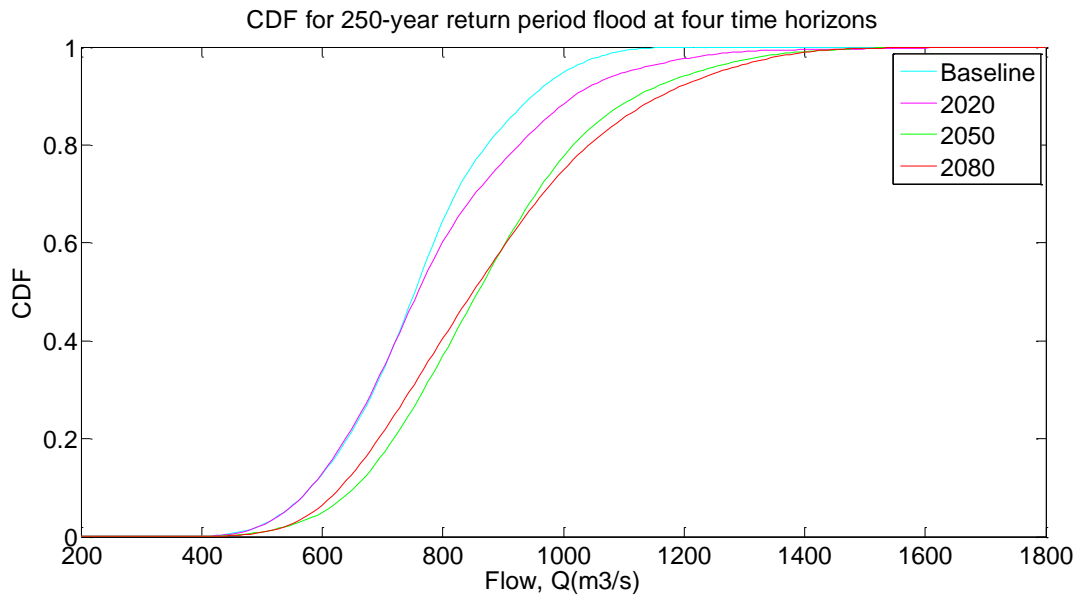


Figure 5.17 CDFs for 250-year return period flood for the four time horizons.

From the results of flood magnitude – return period relationship (Q-T) it can be said that there is significant variability between AOGCMs, and this variability increases when an attempt is made to project flood events for a more distant future. For this reason, climate change impact studies based on only one AOGCM and/or SRES should be considered with a great care. The use of two carefully chosen climate projections (dry and wet projections, for example) may be more appropriate for climate change impact analyses and this has been done in several recent studies (e.g. Prodanovic and Simonovic, 2006).

One of the limitations to the approach presented in this paper is linked to hydrologic model calibration. In this research no attempt has been made to recalibrate the model. The approach implicitly assumes that the calibration is equally acceptable for the baseline and the future conditions. Therefore the focus of future work should be on the expected % changes of design flood magnitude between future climate and baseline period. Based on the percentage changes of design flood magnitude between future climate and baseline period it can be recommended that design extreme floods (i.e. 250-year return period flood) established from observed data should be increased for at least 30% to account for climate change for engineering practice.

## 6 Conclusions

This study uses a multi-model, multi-projection approach to generate probability distribution functions of future extreme flood flows. A wide range of climate model scenarios is used to investigate the climate change related uncertainty in the flood flows for the Upper Thames River basin (Ontario, Canada). Fifteen different climate model scenarios from a combination of six Atmosphere-Ocean Global Climate Models (AOGCMs) and three emission scenarios “A1B”, “B1” and “A2” are used to determine an uncertainty envelope. To account for the natural variability of the hydroclimatic system, a stochastic weather generator was employed to construct sequences of daily precipitation amounts and minimum and maximum air temperatures. A total of 375 (15 AOGCMs X 25 model runs) climate scenarios were produced for the future time horizons centred on 2020, 2050 and 2080 and 25 for baseline period (1979-2005). A continuous daily hydrologic model, calibrated for the basin, was then used to generate daily flow series for the baseline period and for the future time horizons. A peak-over-threshold (POT) modeling approach with Generalized Pareto Distribution is used to produce flood frequency curves for the four time horizons. The uncertainty involved with the POT modelling is also considered. The following conclusions are obtained from the study:

1. Analyzing the shape parameter for the GPD for different datasets, it appears that the POT modelling with GPD using  $k = 0$  (i.e. Exponential distribution) can be used for flood frequency analysis at the Byron gauging station in the Upper Thames River basin.
2. A large uncertainty exists in all the projected future design floods. Use of probabilistic approach helps to better define the uncertainty linked to future climate.
3. Based on the study results, it is reasonable to say that the hydrologic behaviour of the Upper Thames River basin would be modified over the next century. While it is impossible to predict the future flows accurately, the recommendation of this study is to include the uncertainty associated with future design floods into engineering and

management practices. Based on the comparison made with the baseline period it is recommended, for engineering practice that design extreme floods established from observed data should be increased for at least 30% to account for climate change.

## **Acknowledgements**

The authors would like to acknowledge the financial support made available by the Canadian Foundation for Climate and Atmospheric Sciences. Special appreciation is extended to Ms. Leanna King for providing the R-code of weather generator algorithm.

## References

- Beard, LR. 1974. Flood Flow Frequency Techniques, Tech. Report CRWR119, Center for Research in Water Resources, University of Texas at Austin, Austin, TX, USA.
- Bennett, T. 1998. Development and application of a continuous soil moisture accounting algorithm for the Hydrologic Engineering Center Hydrologic Modeling System (HEC-HMS). Masters Thesis, Department of Civil and Environmental Engineering, University of California, Davis, California
- Cunnane, C. 1979. A note on the Poisson assumption in partial duration series models. *Water Resour. Res.* 15 (2), 489–494.
- Cunnane, C. 1973. A particular comparison of annual maxima and partial duration series methods of flood frequency prediction. *J. Hydrol.*, 18: 257-271.
- Cunnane, C. 1989. Statistical distributions for flood frequency analysis. Operational Hydrology Report no. 33, World Meteorological Organization, Geneva.
- Cunderlik, J. M., and Simonovic, S. P. 2004. Assessment of water resources risk and vulnerability to changing climatic conditions: Calibration, verification and sensitivity analysis of the HEC-HMS hydrologic model. Report No. IV, Department of Civil and Environmental Engineering, The University of Western Ontario, London, Ontario, Canada.
- Cunderlik, J. M. and Simonovic, S. P. 2005. Hydrological extremes in a southwestern Ontario river watershed under future climate conditions. *IAHS Hydrological Sciences Journal*, 50(4): 631–654.
- Das, S. 2010. Examination of flood estimation techniques in the Irish context. Ph.D. thesis, Department of Engineering Hydrology, NUI Galway, 2010, available from <http://hdl.handle.net/10379/1688> [accessed: 07 Oct 2011].
- Das, S. and Cunnane, C. 2011. Examination of homogeneity of selected Irish pooling groups. *Hydrol. Earth Syst. Sci.*, 15: 819-830, doi:10.5194/hess-15-819-2011.
- Dalrymple, T., 1960. Flood frequency analysis. US Geological Survey water supply paper No 1534A. 60 p.
- EC 2007. Climate Change and Extreme Rainfall-related Flooding and Surface Runoff Risks in Ontario. Plain Language Summary Report, C.S Cheng, G. Li, Q. Li, H. Auld, D. MacIver, Environment Canada, 18 pages.

- Eum, H.I., Arunachalam, V. and Simonovic, S.P. 2009. Integrated Reservoir Management System for Adaptation to Climate Change Impacts in the Upper Thames River Basin. Water Resources Research Report no. 062, Facility for Intelligent Decision Support, Department of Civil and Environmental Engineering, London, Ontario, Canada, 81 pages.
- Greenwood, J.A., Landwehr, J.M., Matalas, N.C. and Wallis, J.R. 1979. Probability weighted moments - definition and relation to parameters of several distributions expressible in inverse form. *Water Resources Research*, 15(5):1049–1054.
- Ghosh, S., and Majumdar P. P. 2007. Nonparametric methods for modeling GCM and scenario uncertainty in drought assessment, *Water Resources Research*, 43, W07495, 19pp., doi:10.1029/2006WR005351.
- Giorgi, F., and Mearns L. O. 2003. Probability of regional climate change calculated using the reliability ensemble averaging (REA) method, *Geophysical Research Letters*, 30(12), 1629, doi: 10.1029/2003GL017130.
- Hosking, J.R.M. 1990. L-moments: Analysis and estimation of distributions using linear combinations of order statistics. *Journal of the Royal Statistical Society, Series B*, 52, 105–24.
- Hosking, J.R.M. and Wallis, J.R. 1997. *Regional frequency analysis: an approach based on L-moments*. Cambridge University Press, Cambridge.
- Hughes, J. P., and Guttorp P. 1994. A class of stochastic models for relating synoptic atmospheric patterns to regional hydrologic phenomena, *Water Resources Research*, 30(5), 1535–1546.
- IPCC 2007. *Climate Change 2007: Impacts, Adaptation and Vulnerability*. Contribution of Working Group II to the Fourth Assessment Report of the Intergovernmental Panel on Climate Change. Edited by M. Parry et al., Cambridge University Press, UK.
- Kay A , Davies H , Bell V , Jones R. 2009. Comparison of uncertainty sources for climate change impacts: flood frequency in England. *Climatic Change* 92: 41 – 63.
- Kay AL, Jones RG, Reynard NS. 2006a. RCM rainfall for UK flood frequency estimation. I. Climate change results. *Journal of Hydrology* 318: 163 – 172, DOI : 10.1016/j.jhydrol.2005.06.013 .
- Kay AL , Reynard NS, Jones RG. 2006b. RCM rainfall for UK flood frequency estimation. I. Method and validation. *Journal of Hydrology* 318: 151 – 162, DOI : 10.1016/j.jhydrol.2005.06.012 .
- Lang et al., 1999 M. Lang, T.B.M.J. Ouarda, B. Bobée 1999. Towards operational guidelines for over-threshold modelling *Journal of Hydrology*, 225, pp. 103–117.
- Leavesley, G. H. and Stannard, L. G. 1995. The precipitation – runoff modeling system – PRMS, Chapter 9 in *Computer models of watershed hydrology*, V. P. Singh (ed.), Water Resources Publications.

- Leanna King, Tarana Solaiman, and Slobodan P. Simonovic (2009). Assessment of Climatic Vulnerability in the Upper Thames River Basin. Water Resources Research Report no. 064, Facility for Intelligent Decision Support, Department of Civil and Environmental Engineering, London, Ontario, Canada, 61pages. ISBN: (print) 978-0-7714-2816-6; (online) 978-0-7714-2817-3.
- Loukas A , Vasiliades L , Dalezios NR. 2002. Potential climate change impacts on flood producing mechanisms in southern British Columbia, Canada using the CGCMA1 simulation results. *Journal of Hydrology* 259: 163 – 188, DOI : P ii S0022- 1694( 01) 00580- 7.
- Mareuil A , Leconte R, Brissette F, Minville M. 2007. Impacts of climate change on the frequency and severity of floods in the Chateauguay River basin, Canada. *Canadian Journal of Civil Engineering* 34: 1048 – 1060, DOI : 10.1139/107- 022.
- Minville, M., Brissette, F., Leconte, R. 2008. Uncertainty of the impact of climate change on the hydrology of a nordic watershed. *Journal of Hydrology*, vol 358, n1-2, 2008, p 70-83
- NERC 1975. Flood Studies Report. Nat. Environ. Res. Council, Vol I, London, UK.
- Nakićenović, N., and Swart, R. (eds.) 2000. Special Report on Emissions Scenarios. A Special Report of Working Group III of the Intergovernmental Panel on Climate Change. Cambridge University Press, Cambridge, United Kingdom and New York, NY, USA, 599 pp.
- Pickands, J., 1975. Statistical inference using extreme order statistics. *Ann. Stat.* 3 (1), 119–131.
- Prudhomme, Christel, Jakob, Dorte, Svensson, Cecilia, 2003. Uncertainty and climate change impact on the flood regime of small UK catchments. *Journal of Hydrology* 277, 1–23.
- PIEVC 2008. Adapting to Climate Change, Canada’s First National Engineering Vulnerability Assessment of Public Infrastructure .Canadian Council of Professional Engineers.
- Prodanovic, P. and S. P. Simonovic, 2006. Inverse drought risk modeling of the Upper Thames River Watershed. Water Resources Research Report no. 053, Facility for Intelligent Decision Support, Department of Civil and Environmental Engineering, London, Ontario, Canada, 252 pages. ISBN: (print) 978-0-7714-2636-0; (online) 978-0-7714-2637-7.
- Prodanovic, P., and Simonovic, S.P. 2007. Development of rainfall intensity duration frequency curves for the City of London under the changing climate. Water Resources Research Report no. 058, Facility for Intelligent Decision Support, Department of Civil and Environmental Engineering, London, Ontario, Canada, 51 pages.
- Rosbjerg, D, Madsen, H and Rasmussen, PF. 1992. Prediction in Partial Duration Series with Generalized Pareto-Distributed Exceedances, *Water Resources Research*, 28(11):3001-3010.
- Roy, Luc, Brissette, Francois, Leconte, Robert, Marche, Claude, 2001. The impact of climate change on seasonal floods of a southern Quebec River Basin. *Hydrological Processes* 15, 3167–3179.

- Sharif, M., and Burn, D.H. 2006. Simulating climate change scenarios using an improved K-nearest neighbor model. *Journal of hydrology*, 325: 179-196.
- Simonovic, S.P. 2008. Engineering literature review: water resources — infrastructure impacts, vulnerabilities and design considerations for future climate change. In *Adapting to Climate Change, Canada's First National Engineering Vulnerability Assessment of Public Infrastructure — Appendix C Literature Reviews*. Engineers Canada.
- Solaiman, T.A., and Simonovic, S.P. 2011. Development of Probability Based Intensity-Duration-Frequency Curves under Climate Change, *Water Resources Research Report no. 072*, Facility for Intelligent Decision Support, Department of Civil and Environmental Engineering, London, Ontario, Canada, 93 pages.
- Smith, R. L., C. Tebaldi, D. Nychka, and L. Mearns, 2009. Bayesian modeling of uncertainty in ensembles of climate models, *Journal of the American Statistical Association*, 104 (485), 97-116., doi:10.1198/jasa.2009.0007.
- Tebaldi, C., L. O. Mearns, D. Nychka, and R. L. Smith, 2004. Regional probabilities of precipitation change: A Bayesian analysis of multimodel simulations, *Geophysical Research Letters*, 31.
- Tebaldi, C., R. L. Smith, D. Nychka and L.O. Mearns, 2005. Quantifying uncertainty in Projections of Regional Climate Change: a Bayesian Approach to the Analysis of Multimodel Ensembles, *Journal of Climate*, 18 (10), 1524-1540.
- USACE 2000. Hydrologic Modelling System HEC-HMS. Technical reference manual, United States Army Corps of Engineers, Hydrologic Engineering Center, Davis, California.
- USACE 2006. Hydrologic Modelling System HEC-HMS, User's manual for version 3.0.1. United States Army Corps of Engineers, Hydrologic Engineering Center, Davis, California.
- Wang, Q.J., 1991. The POT model described by the generalized Pareto distribution with Poisson arrival rate. *J. Hydrol.* 129, 263–280.
- Willems P. 2003. WETSPRO: Water Engineering Time Series PROcessing tool tool, Reference Manual and User's Manual, Hydraulics Laboratory K.U.Leuven, Leuven, Belgium.
- Willems, P. 2008. A time series tool to support the multi-criteria performance evaluation of rainfall-runoff models, *Environ. Model. Softw.* , doi:10.1016/j.envsoft.2008.09.005

## APPENDIX A

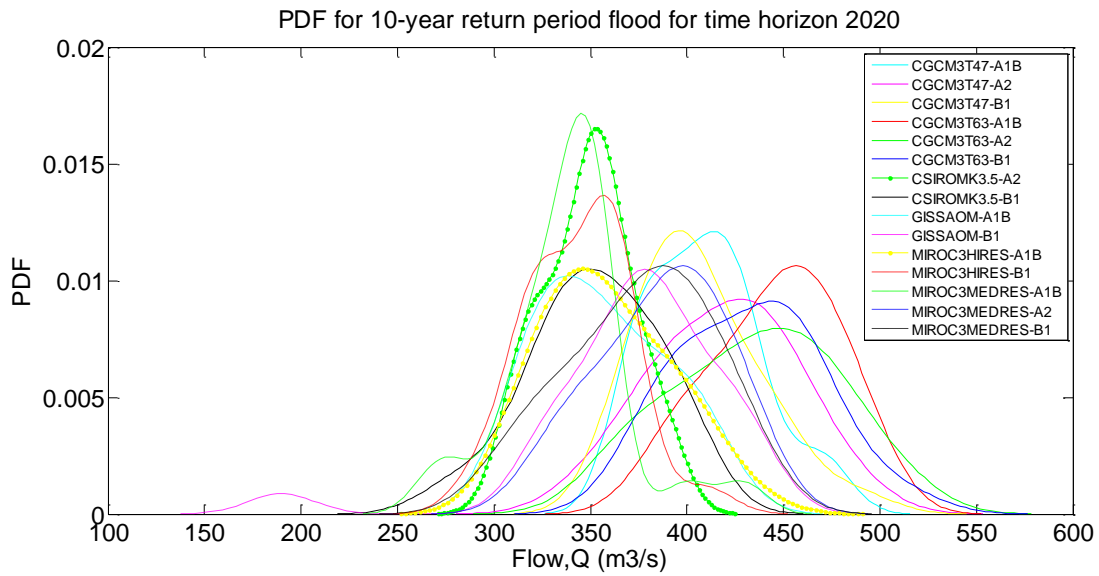


Figure A. 1 Probability density functions for 10-year return period flood for all climate model scenarios at the time horizon 2020.

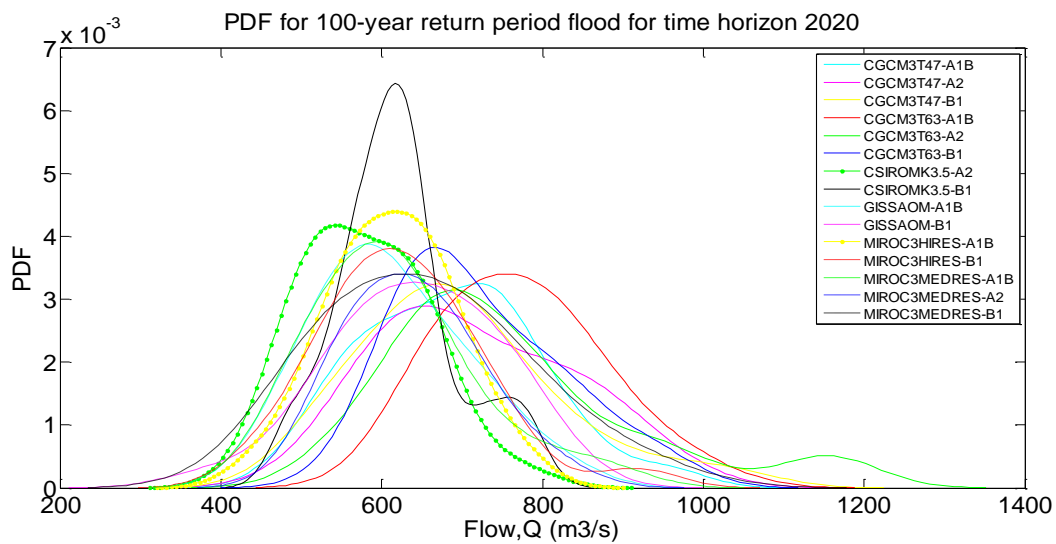


Figure A. 2 Probability density functions for 100-year return period flood for all climate model scenarios at the time horizon 2020.

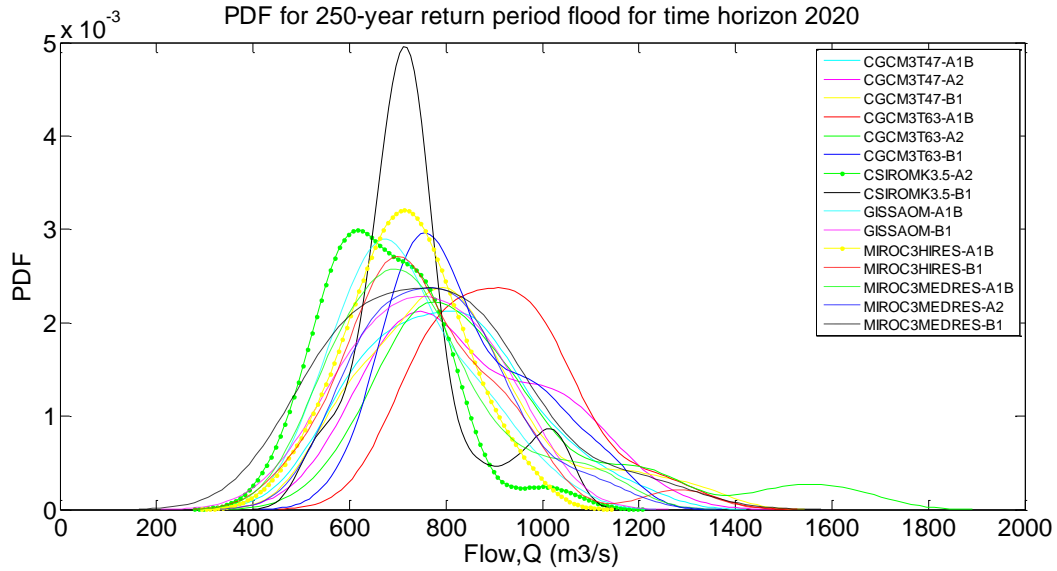


Figure A. 3 Probability density functions for 250-year return period flood for all climate model scenarios at the time horizon 2020.

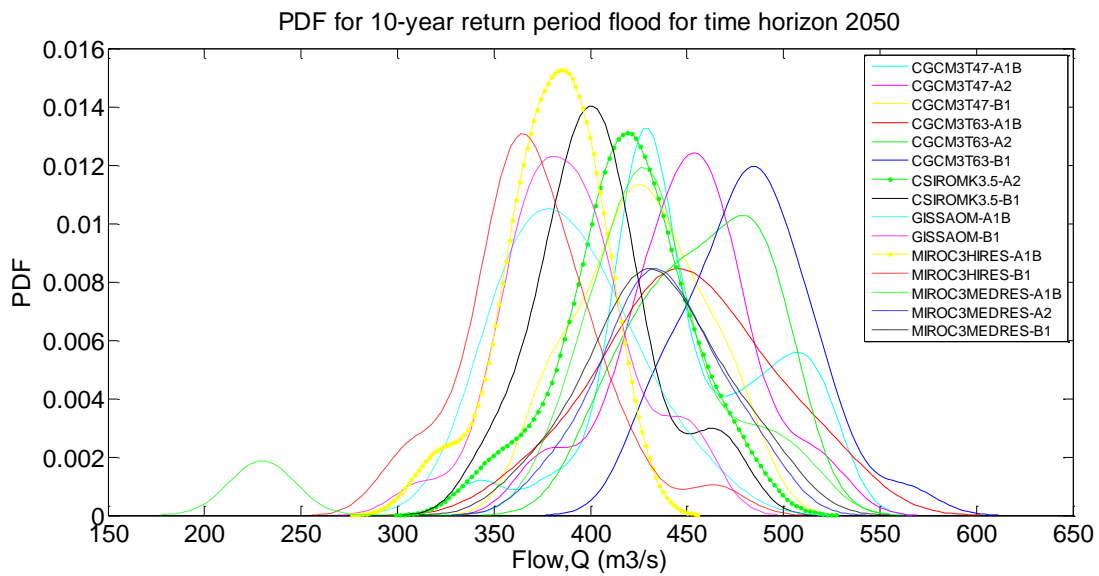


Figure A. 4 Probability density functions for 10-year return period flood for all climate model scenarios at the time horizon 2050.

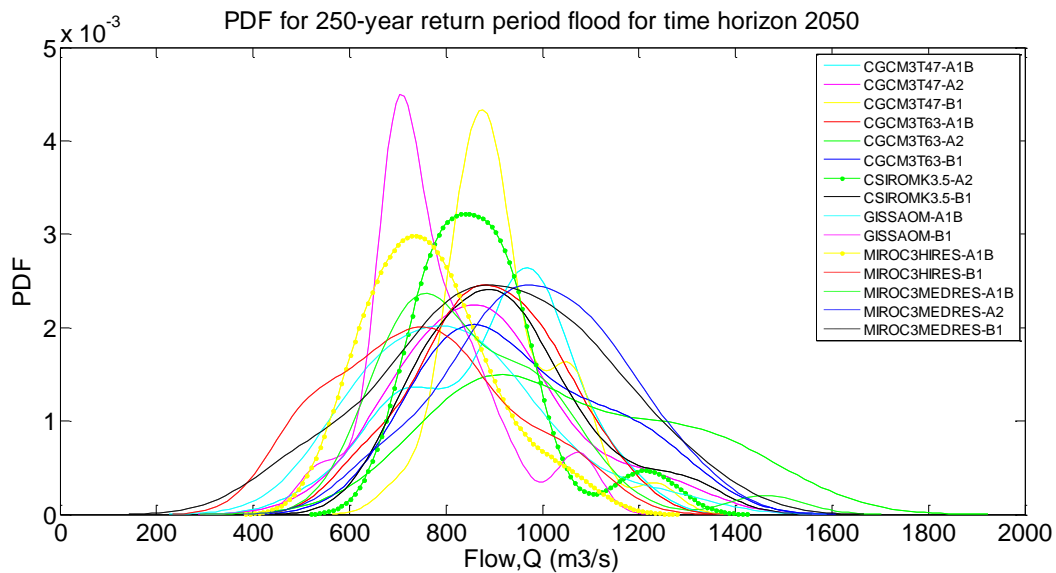


Figure A. 5 Probability density functions for 250-year return period flood for all climate model scenarios at the time horizon 2050.

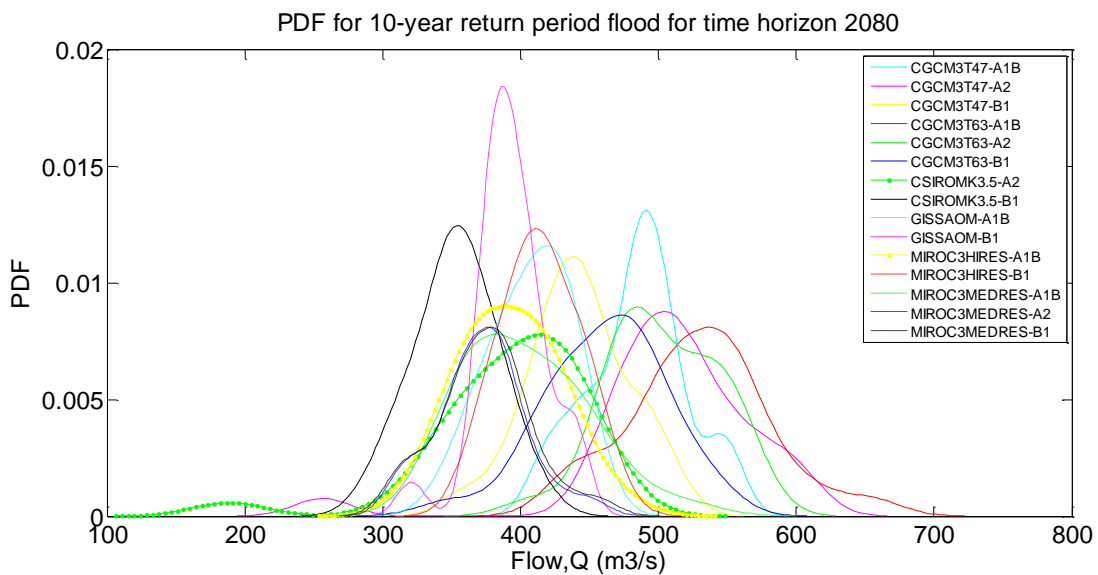


Figure A. 6 Probability density functions for 10-year return period flood for all climate model scenarios at the time horizon 2080.

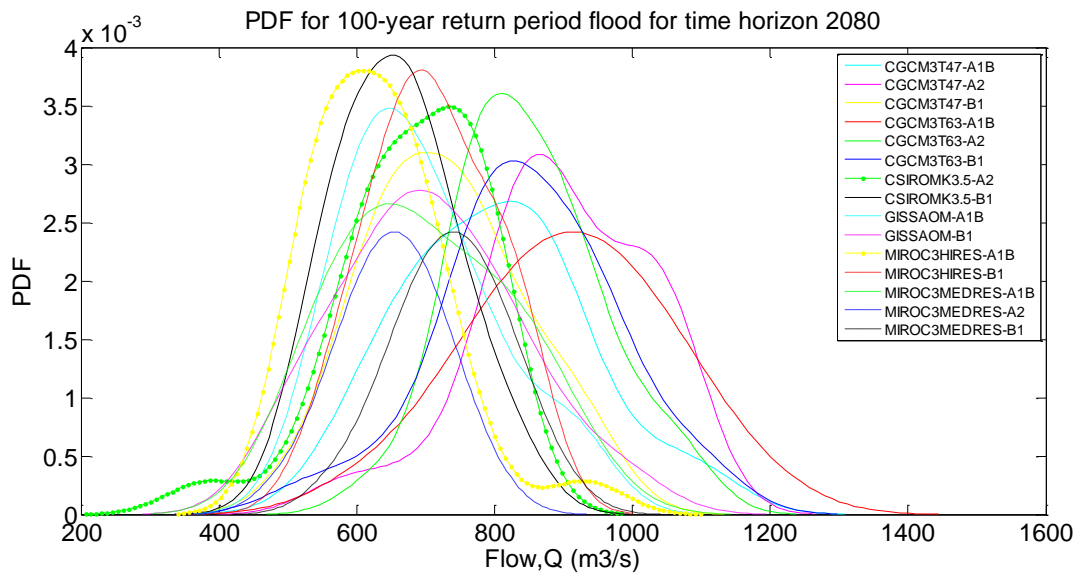


Figure A. 7 Probability density functions for 100-year return period flood for all climate model scenarios at the time horizon 2080.

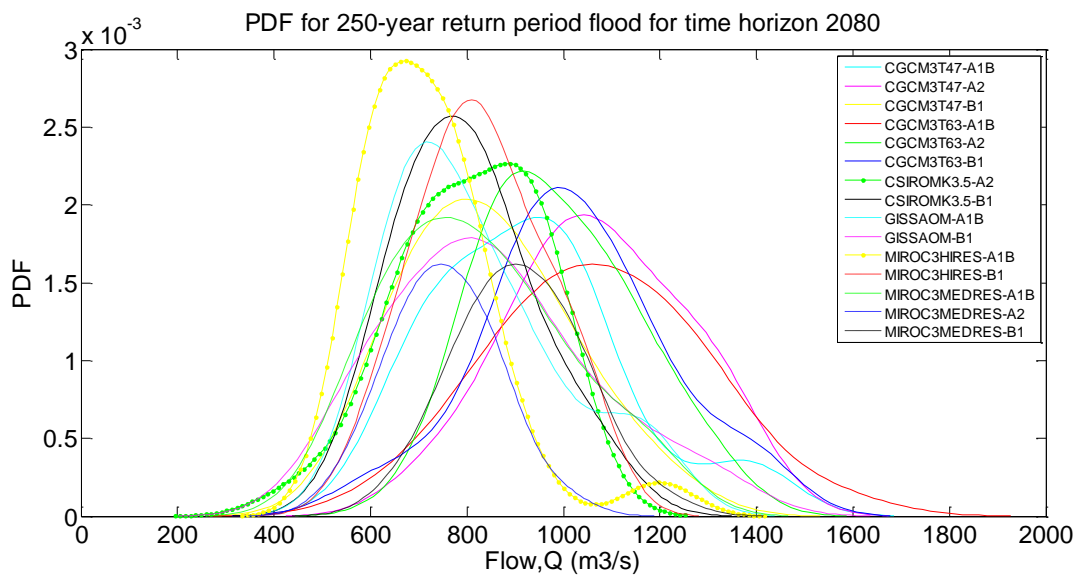


Figure A. 8 Probability density functions for 250-year return period flood for all climate model scenarios at the time horizon 2080.

## **APPENDIX B**

### **List of Previous Reports in the Series**

ISSN: (print) 1913-3200; (online) 1913-3219

(1) Slobodan P. Simonovic (2001). Assessment of the Impact of Climate Variability and Change on the Reliability, Resiliency and Vulnerability of Complex Flood Protection Systems. Water Resources Research Report no. 038, Facility for Intelligent Decision Support, Department of Civil and Environmental Engineering, London, Ontario, Canada, 91 pages. ISBN: (print) 978-0-7714-2606-3; (online) 978-0-7714-2607-0.

(2) Predrag Prodanovic (2001). Fuzzy Set Ranking Methods and Multiple Expert Decision Making. Water Resources Research Report no. 039, Facility for Intelligent Decision Support, Department of Civil and Environmental Engineering, London, Ontario, Canada, 68 pages. ISBN: (print) 978-0-7714-2608-7; (online) 978-0-7714-2609-4.

(3) Nirupama and Slobodan P. Simonovic (2002). Role of Remote Sensing in Disaster Management. Water Resources Research Report no. 040, Facility for Intelligent Decision Support, Department of Civil and Environmental Engineering, London, Ontario, Canada, 107 pages. ISBN: (print) 978-0-7714-2610-0; (online) 978-0-7714-2611-7.

(4) Taslima Akter and Slobodan P. Simonovic (2002). A General Overview of Multiobjective Multiple-Participant Decision Making for Flood Management. Water Resources Research Report no. 041, Facility for Intelligent Decision Support, Department of Civil and Environmental Engineering, London, Ontario, Canada, 65 pages. ISBN: (print) 978-0-7714-2612-4; (online) 978-0-7714-2613-1.

(5) Nirupama and Slobodan P. Simonovic (2002). A Spatial Fuzzy Compromise Approach for Flood Disaster Management. Water Resources Research Report no. 042, Facility for Intelligent Decision Support, Department of Civil and Environmental Engineering, London, Ontario, Canada, 138 pages. ISBN: (print) 978-0-7714-2614-8; (online) 978-0-7714-2615-5.

(6) K. D. W. Nandalal and Slobodan P. Simonovic (2002). State-of-the-Art Report on Systems Analysis Methods for Resolution of Conflicts in Water Resources Management. Water Resources Research Report no. 043, Facility for Intelligent Decision Support, Department of Civil and Environmental Engineering, London, Ontario, Canada, 216 pages. ISBN: (print) 978-0-7714-2616-2; (online) 978-0-7714-2617-9.

(7) K. D. W. Nandalal and Slobodan P. Simonovic (2003). Conflict Resolution Support System – A Software for the Resolution of Conflicts in Water Resource Management. Water Resources Research Report no. 044, Facility for Intelligent Decision Support, Department of Civil and Environmental Engineering, London, Ontario, Canada, 144 pages. ISBN: (print) 978-0-7714-2618-6; (online) 978-0-7714-2619-3.

- (8) Ibrahim El-Baroudy and Slobodan P. Simonovic (2003). New Fuzzy Performance Indices for Reliability Analysis of Water Supply Systems. Water Resources Research Report no. 045, Facility for Intelligent Decision Support, Department of Civil and Environmental Engineering, London, Ontario, Canada, 90 pages. ISBN: (print) 978-0-7714-2620-9; (online) 978-0-7714- 2621-6.
- (9) Juraj Cunderlik (2003). Hydrologic Model Selection for the CFCAS Project: Assessment of Water Resources Risk and Vulnerability to Changing Climatic Conditions. Water Resources Research Report no. 046, Facility for Intelligent Decision Support, Department of Civil and Environmental Engineering, London, Ontario, Canada, 40 pages. ISBN: (print) 978-0-7714- 2622-3; (online) 978-0-7714- 2623-0.
- (10) Juraj Cunderlik and Slobodan P. Simonovic (2004). Selection of Calibration and Verification Data for the HEC-HMS Hydrologic Model. Water Resources Research Report no. 047, Facility for Intelligent Decision Support, Department of Civil and Environmental Engineering, London, Ontario, Canada, 29 pages. ISBN: (print) 978-0-7714-2624-7; (online) 978-0-7714-2625-4.
- (11) Juraj Cunderlik and Slobodan P. Simonovic (2004). Calibration, Verification and Sensitivity Analysis of the HEC-HMS Hydrologic Model. Water Resources Research Report no. 048, Facility for Intelligent Decision Support, Department of Civil and Environmental Engineering, London, Ontario, Canada, 113 pages. ISBN: (print) 978- 0-7714-2626-1; (online) 978-0-7714- 2627-8.
- (12) Predrag Prodanovic and Slobodan P. Simonovic (2004). Generation of Synthetic Design Storms for the Upper Thames River basin. Water Resources Research Report no. 049, Facility for Intelligent Decision Support, Department of Civil and Environmental Engineering, London, Ontario, Canada, 20 pages. ISBN: (print) 978- 0-7714-2628-5; (online) 978-0-7714-2629-2.
- (13) Ibrahim El-Baroudy and Slobodan P. Simonovic (2005). Application of the Fuzzy Performance Indices to the City of London Water Supply System. Water Resources Research Report no. 050, Facility for Intelligent Decision Support, Department of Civil and Environmental Engineering, London, Ontario, Canada, 137 pages. ISBN: (print) 978-0-7714-2630-8; (online) 978-0-7714-2631-5.
- (14) Ibrahim El-Baroudy and Slobodan P. Simonovic (2006). A Decision Support System for Integrated Risk Management. Water Resources Research Report no. 051, Facility for Intelligent Decision Support, Department of Civil and Environmental Engineering, London, Ontario, Canada, 146 pages. ISBN: (print) 978-0-7714-2632-2; (online) 978-0-7714-2633-9.
- (15) Predrag Prodanovic and Slobodan P. Simonovic (2006). Inverse Flood Risk Modelling of The Upper Thames River Basin. Water Resources Research Report no. 052, Facility for Intelligent Decision Support, Department of Civil and Environmental Engineering, London, Ontario, Canada, 163 pages. ISBN: (print) 978-0-7714-2634-6; (online) 978-0-7714-2635-3.

(16) Predrag Prodanovic and Slobodan P. Simonovic (2006). Inverse Drought Risk Modelling of The Upper Thames River Basin. Water Resources Research Report no. 053, Facility for Intelligent Decision Support, Department of Civil and Environmental Engineering, London, Ontario, Canada, 252 pages. ISBN: (print) 978-0-7714-2636-0; (online) 978-0-7714-2637-7.

(17) Predrag Prodanovic and Slobodan P. Simonovic (2007). Dynamic Feedback Coupling of Continuous Hydrologic and Socio-Economic Model Components of the Upper Thames River Basin. Water Resources Research Report no. 054, Facility for Intelligent Decision Support, Department of Civil and Environmental Engineering, London, Ontario, Canada, 437 pages. ISBN: (print) 978-0-7714-2638-4; (online) 978-0-7714-2639-1.

(18) Subhankar Karmakar and Slobodan P. Simonovic (2007). Flood Frequency Analysis Using Copula with Mixed Marginal Distributions. Water Resources Research Report no. 055, Facility for Intelligent Decision Support, Department of Civil and Environmental Engineering, London, Ontario, Canada, 144 pages. ISBN: (print) 978-0-7714-2658-2; (online) 978-0-7714-2659-9.

(19) Jordan Black, Subhankar Karmakar and Slobodan P. Simonovic (2007). A Web-Based Flood Information System. Water Resources Research Report no. 056, Facility for Intelligent Decision Support, Department of Civil and Environmental Engineering, London, Ontario, Canada, 133 pages. ISBN: (print) 978-0-7714-2660-5; (online) 978-0-7714-2661-2.

(20) Angela Peck, Subhankar Karmakar and Slobodan P. Simonovic (2007). Physical, Economical, Infrastructural and Social Flood Risk – Vulnerability Analyses in GIS. Water Resources Research Report no. 057, Facility for Intelligent Decision Support, Department of Civil and Environmental Engineering, London, Ontario, Canada, 80 pages. ISBN: (print) 978-0-7714-2662-9; (online) 978-0-7714-2663-6.

(21) Predrag Prodanovic and Slobodan P. Simonovic (2007). Development of Rainfall Intensity Duration Frequency Curves for the City of London Under the Changing Climate. Water Resources Research Report no. 058, Facility for Intelligent Decision Support, Department of Civil and Environmental Engineering, London, Ontario, Canada, 51 pages. ISBN: (print) 978-0-7714-2667-4; (online) 978-0-7714-2668-1.

(22) Evan G. R. Davies and Slobodan P. Simonovic (2008). An integrated system dynamics model for analyzing behaviour of the social-economic-climatic system: Model description and model use guide. Water Resources Research Report no. 059, Facility for Intelligent Decision Support, Department of Civil and Environmental Engineering, London, Ontario, Canada, 233 pages. ISBN: (print) 978-0-7714-2679-7; (online) 978-0-7714-2680-3.

(23) Vasan Arunachalam (2008). Optimization Using Differential Evolution. Water Resources Research Report no. 060, Facility for Intelligent Decision Support, Department of Civil and Environmental Engineering, London, Ontario, Canada, 42 pages. ISBN: (print) 978-0-7714-2689-6; (online) 978-0-7714-2690-2.

(24) Rajesh Shrestha and Slobodan P. Simonovic (2009). A Fuzzy Set Theory Based Methodology for Analysis of Uncertainties in Stage-Discharge Measurements and Rating Curve. Water Resources Research Report no. 061,

Facility for Intelligent Decision Support, Department of Civil and Environmental Engineering, London, Ontario, Canada, 104 pages. ISBN: (print) 978-0-7714-2707-7; (online) 978-0-7714-2708-4.

(25) Hyung-II Eum, Vasana Arunachalam and Slobodan P. Simonovic (2009). Integrated Reservoir Management System for Adaptation to Climate Change Impacts in the Upper Thames River Basin. Water Resources Research Report no. 062, Facility for Intelligent Decision Support, Department of Civil and Environmental Engineering, London, Ontario, Canada, 81 pages. ISBN: (print) 978-0-7714-2710-7; (online) 978-0-7714-2711-4.

(26) Evan G. R. Davies and Slobodan P. Simonovic (2009). Energy Sector for the Integrated System Dynamics Model for Analyzing Behaviour of the Social- Economic-Climatic Model. Water Resources Research Report no. 063. Facility for Intelligent Decision Support, Department of Civil and Environmental Engineering, London, Ontario, Canada. 191 pages. ISBN: (print) 978-0-7714-2712-1; (online) 978-0-7714-2713-8.

(27) Leanna King, Tarana Solaiman, and Slobodan P. Simonovic (2009). Assessment of Climatic Vulnerability in the Upper Thames River Basin. Water Resources Research Report no. 064, Facility for Intelligent Decision Support, Department of Civil and Environmental Engineering, London, Ontario, Canada, 61pages. ISBN: (print) 978-0-7714-2816-6; (online) 978-0-7714- 2817-3.

(28) Slobodan P. Simonovic and Angela Peck (2009). Updated Rainfall Intensity Duration Frequency Curves for the City of London under Changing Climate. Water Resources Research Report no. 065, Facility for Intelligent Decision Support, Department of Civil and Environmental Engineering, London, Ontario, Canada, 64pages. ISBN: (print) 978-0-7714-2819-7; (online) 978-0-7714-2820-3.

(29) Leanna King, Tarana Solaiman, and Slobodan P. Simonovic (2010). Assessment of Climatic Vulnerability in the Upper Thames River Basin: Part 2. Water Resources Research Report no. 066, Facility for Intelligent Decision Support, Department of Civil and Environmental Engineering, London, Ontario, Canada, 72pages. ISBN: (print) 978-0-7714-2834-0; (online) 978-0-7714-2835-7.

(30) Christopher J. Popovich, Slobodan P. Simonovic and Gordon A. McBean (2010). Use of an Integrated System Dynamics Model for Analyzing Behaviour of the Social-Economic-Climatic System in Policy Development. Water Resources Research Report no. 067, Facility for Intelligent Decision Support, Department of Civil and Environmental Engineering, London, Ontario, Canada, 37 pages. ISBN: (print) 978-0-7714-2838-8; (online) 978-0-7714-2839-5.

(31) Hyung-II Eum and Slobodan P. Simonovic (2009). City of London: Vulnerability of Infrastructure to Climate Change; Background Report 1 – Climate and Hydrologic Modeling. Water Resources Research Report no. 068, Facility for Intelligent Decision Support, Department of Civil and Environmental Engineering, London, Ontario, Canada, 102pages. ISBN: (print) 978-0-7714-2844-9; (online) 978-0-7714-2845-6.

(32) Dragan Sredojevic and Slobodan P. Simonovic (2009). City of London: Vulnerability of Infrastructure to Climate Change; Background Report 2 – Hydraulic Modeling and Floodplain Mapping. Water Resources Research

Report no. 069, Facility for Intelligent Decision Support, Department of Civil and Environmental Engineering, London, Ontario, Canada, 147 pages. ISBN: (print) 978-0-7714-2846-3; (online) 978-0-7714-2847-0.

(33) Tarana A. Solaiman and Slobodan P. Simonovic (2011). Quantifying Uncertainties in the Modelled Estimates of Extreme Precipitation Events at the Upper Thames River Basin. Water Resources Research Report no. 070, Facility for Intelligent Decision Support, Department of Civil and Environmental Engineering, London, Ontario, Canada, 167 pages. ISBN: (print) 978-0-7714-2878-4; (online) 978-0-7714-2880-7.

(34) Tarana A. Solaiman and Slobodan P. Simonovic (2011). Assessment of Global and Regional Reanalyses Data for Hydro-Climatic Impact Studies in the Upper Thames River Basin. Water Resources Research Report no. 071, Facility for Intelligent Decision Support, Department of Civil and Environmental Engineering, London, Ontario, Canada, 74 pages. ISBN: (print) 978-0-7714-2892-0; (online) 978-0-7714-2899-9.

(35) Tarana A. Solaiman and Slobodan P. Simonovic (2011). Development of Probability Based Intensity-Duration-Frequency Curves under Climate Change. Water Resources Research Report no. 072, Facility for Intelligent Decision Support, Department of Civil and Environmental Engineering, London, Ontario, Canada, 89 pages. ISBN: (print) 978-0-7714-2893-7; (online) 978-0-7714-2900-2.

(36) Dejan Vucetic and Slobodan P. Simonovic (2011). Water Resources Decision Making Under Uncertainty. Water Resources Research Report no. 073, Facility for Intelligent Decision Support, Department of Civil and Environmental Engineering, London, Ontario, Canada, 143 pages. ISBN: (print) 978-0-7714-2894-4; (online) 978-0-7714-2901-9.

(37) Angela Peck, Elisabeth Bowering and Slobodan P. Simonovic (2010). City of London: Vulnerability of Infrastructure to Climate Change, Final Report - Risk Assessment. Water Resources Research Report no. 074, Facility for Intelligent Decision Support, Department of Civil and Environmental Engineering, London, Ontario, Canada, 66 pages. ISBN: (print) 978-0-7714-2895-1; (online) 978-0-7714-2902-6.

(38) Akhtar, M. K., S. P. Simonovic, J. Wibe, J. MacGee, and J. Davies, (2011). An integrated system dynamics model for analyzing behaviour of the social-energy-economic-climatic system: model description. Water Resources Research Report no. 075, Facility for Intelligent Decision Support, Department of Civil and Environmental Engineering, London, Ontario, Canada, 211 pages. ISBN: (print) 978-0-7714-2896-8; (online) 978-0-7714-2903-3.

(39) Akhtar, M. K., S. P. Simonovic, J. Wibe, J. MacGee, and J. Davies, (2011). An integrated system dynamics model for analyzing behaviour of the social-energy-economic-climatic system: user's manual. Water Resources Research Report no. 076, Facility for Intelligent Decision Support, Department of Civil and Environmental Engineering, London, Ontario, Canada, 161 pages. ISBN: (print) 978-0-7714-2897-5; (online) 978-0-7714-2904-0.

(40) Millington, N., S. Das and S. P. Simonovic (2011). The Comparison of GEV, Log-Pearson Type 3 and Gumbel Distributions in the Upper Thames River Watershed under Global Climate Models. Water Resources Research

Report no. 077, Facility for Intelligent Decision Support, Department of Civil and Environmental Engineering, London, Ontario, Canada, 53 pages. ISBN: (print) 978-0-7714-2898-2; (online) 978-0-7714-2905-7.

(41) Andre Schardong and Slobodan P. Simonovic (2011). Multi-objective Evolutionary Algorithms for Water Resources Management. Water Resources Research Report no. 078, Facility for Intelligent Decision Support, Department of Civil and Environmental Engineering, London, Ontario, Canada, 167 pages. ISBN: (print) 978-0-7714-2907-1; (online) 978-0-7714-2908-8.